Beams-doc-3248

Proposal for Experiments and Upgrades at the A0 Photoinjector

Editor: Mike Church

Contributors: Leo Bellantoni, Nathan Eddy, Don Edwards, Helen Edwards, Ralph Fiorito, Ray Fliller, Elvin Harms, Grigory Kazakevich, Tim Koeth, Alex Lumpkin, Sergei Nagaitsev, Philippe Piot, Jinhao Ruan, Vic Scarpine, Bill Soyars, Yin-e Sun, Mike Syphers, Randy Thurman-Keup, Manfred Wendt

November 10, 2008

Table of Contents

1 Introduction

The Fermilab A0 photoinjector (A0PI) is a 16 MeV electron linac located in the A0 service building above the Tevatron beam enclosure. Since 1992 it has been used for accelerator research and training in the development and operation of electron injectors, lasers, and superconducting RF systems [1]. The photoinjector consists of a 1.3 GHz normal conducting RF gun with a Cs_2Te photocathode, a low gradient 1.3 GHz TESLA technology "capture" cavity, a transport channel for experiments and diagnostics, a 45° bend to a dump, and a user experimental area. The beam parameters and the current beamline layout are shown in Appendices 6.1 and 6.2, respectively.

The injector can be configured to provide both compressed and uncompressed beam. The bunch structure of the beam is similar to the TESLA Test Facility at DESY, with 1 μs bunch spacing and bunch trains up to 200 μs duration. Bunch charge up to 10 nC has been available, and such high charge bunches have been used in successful plasma wakefield experiments [2].

Another area of focus has been round-to-flat beam transformation experiments in which equal emittances in the two transverse planes are repartitioned to give a very large relative ratio of 100:1. This experiment required the addition of a three quadrupole "transformer" and the ability to provide magnetic field (B_z) on the cathode. It was completed in 2005 [3]. Other experiments at this time included the characterization of the bunch compression with two macroparticles [4].

The present ongoing experiment attempts to perform efficient emittance exchange between the longitudinal plane and one transverse plane. This experiment has required a reconfiguration of the beam line. The magnetic chicane was removed and reconfigured into a two dogleg arrangement with a deflecting mode cavity after the first dogleg. The deflecting mode cavity was previously developed in a superconducting version for an HEP experiment [5]. The emittance exchange experiment, with its very short bunch lengths, has reemphasized the need for developing better methods of bunch length measurement. Present experiments typically use 1 nC bunch charge, and at this intensity coherent synchrotron radiation (CSR) can be important.

This proposal addresses the following experimental themes.

<u>Theme 1: Generation, transport, and manipulation of high-brightness electron beams</u>

The next generation of the emittance exchange experiment will focus on emittance measurements after the exchange for different initial transverse and longitudinal phase space configurations and bunch charges. Emittance exchange in combination with flat beam transforms can possibly be a path to providing matched beams for high gain FELs and other applications [6]. The focus will include some investigations into collective effects, which we expect are present. We will also investigate the possibility of bunch train generation at the sub ps level from single bunches. We expect strong collaboration with ANL and NIU on these experiments.

Thee-dimensional ellipsoidal charge distributions produce linear space charge fields within the distribution and are in principle free of space-charge-induced phase space dilution. Beam conditions necessary for ellipsoidal bunch generation can in principle be achieved at the A0PI. The generation of ellipsoidal bunches from magnesium and copper cathodes has been recently demonstrated [7][8], however generating such a distribution out of a high quantum efficiency semiconductor cathode such as Cs_2Te would be an important proof-of-principle experiment,

which we are proposing to do. This technique of generating high brightness electron bunches by photocathodes could benefit several projects [9].

Microbunching of high intensity compressed beams from (presumably) a combination of CSR and space charge effects has recently been identified as a source of error in emittance diagnostics of such beams at a number of electron beam facilities [10]. These effects severely limit the use of many standard beam size diagnostics over a wide range of relevant beam parameters. We are considering a series of experiments to study this effect to further understand it and possibly mitigate it.

A possible longer term theme of emittance manipulation includes the improvement of the round-to-flat beam transformation and its adaptation for use in an image charge undulator. Round-to-flat beam experiments have attained a ratio of 100:1 in the transverse emittance ratio, and we are interested in pushing this ratio even higher.

Transverse adiabatic capture of a ring beam is an accelerator physics concept that has been developed by Y. Derbenev [11] and requires a proof-of-principle experiment. This concept incorporates the flat beam transformation and possibly the emittance exchange. It may provide a path toward developing lower emittance beams at high charge density, and it may help in the goal of developing ILC-like injector parameters. We plan to study how it could be implemented but don't expect to be able to complete this experiment until the photoinjector is moved to the new test accelerator at the New Muon Lab (NML) building.

Theme 2: Diagnostic experiments

There are a number of beam diagnostic instruments that we are currently developing and will continue to develop in the near time scale. In particular, we are developing several promising techniques for bunch length monitoring for very short beams: a non-intercepting technique using electro-optical (EO) sampling; a more standard technique using a deflecting mode cavity; a technique using coherent transition radiation (CTR) from a flat screen radiator; and a technique using Martin-Puplett interferometry.

Theme 3: Technology development

The A0PI group has also been interested in developing a spin polarized RF gun using a GaAs photocathode. This photocathode is extremely sensitive to vacuum conditions in the gun, and to date has only been successfully used in DC guns. Fermilab is collaborating with DULY Research Inc. to produce a Plane Wave Transformer (PWT) gun which has an open RF structure which will allow for greater pumping via a sputtered non-evaporate getter (SNEG) coating. To this end, A0 has a cathode preparation chamber for GaAs photocathodes which has yet to be commissioned. DULY Research Inc is building the gun, and is funded by a Phase II SBIR.

Another technology that may prove useful for a spin polarized electron RF gun is a superconducting RF gun. Such a gun will have excellent vacuum and may support such a cathode. BNL is already pursuing this course, and we hope to leverage our SRF infrastructure to collaborate with them on this project.

LLRF development is a core development for many plans at FNAL. The A0PI with its different cavity systems and beam is an ideal and unique test bed at FNAL for this development.

In addition to near term work on the cathode drive laser and the development of a laser for an EO system, we have plans to become knowledgeable in fiber laser technology as this technology

may provide better and less costly alternatives to today's solutions.

It is worth noting that with a higher energy beam the laser acceleration experiment proposed by Melissinos [12][13] using a ring structure laser would be possible. We are not at this time considering this experiment. Also with our large bunch charge capability (~10 nC), plasma experiments are possible and have been done at the A0PI in the past. We do not plan to pursue these experiments at present as very competitive work is being done elsewhere.

References

[1] *Fermilab NICADD Photoinjector Laboratory*, WWW Document, (http://nicadd.niu.edu/fnpl/).

[2] N. Barov *et al.*, Phys. Rev. ST Accel. Beams **7**, 061301 (2004).

[3] P. Piot *et al.*, Phys. Rev. ST Accel. Beams **9**, 031001 (2006).

[4] R. Tikhoplav *et al.*, "Investigation of the Longitudinal Beam Dynamics in a Photoinjector Using a Two-macroparticle Model", in *Proc. LINAC2004, Lubeck, Germany*.

[5] C. Adolphsen *et al.*, EuroTev Report 2007-10 (2007).

[6] K.-J. Kim, TUYAB01, in *Proc. of PAC2007, Albuquerque, NM*

[7] P. Musumeci, *et al.*, Phys. Rev. Let. **100** (2008).

[8] J. Luiten, *et al.*, in *Proc. 13th Advanced Accelerator Concepts Workshop, Santa Cruz, CA* (2008, to be published).

[9] R. Legg, *et al.*, in *Proc. EPAC2008, Genova, Italy*; W. Graves, private communication.

[10] A.H. Lumpkin, *et al*., "Observation of Enhanced OTR Signals from a Compressed Electron Beam", in *Proc. BIW2008, Lake Tahoe, CA* (to be published).

[11] Y. Derbenev, NIM A **441**, 223 (2000).

[12] R. Tikhoplav *et al.*, in *Proc. of EPAC2002, Paris, France*, p. 984.

[13] P. Piot, A. Melissinos, R. Tikhoplav, in *Proc. of PAC2005, Knoxville, TN*, p. 2503.

2 Beam physics experiments

2.1 Emittance exchange experiments

Transverse to longitudinal emittance exchange was proposed by Y. Orlov et al. in 1991 [1]. In 2002, Cornacchia and Emma proposed an approximate exchange which consists of a dipole mode cavity flanked by two doglegs of opposite sign [2]. K.–J. Kim modified the optics to achieve exact emittance exchange [3]. Based on Kim's optics, a transverse to longitudinal emittance exchange experiment is currently being performed at the A0PI. The goals of the experiment are: demonstrate proof-of-principle, study the dynamics of the exchange, understand emittance diluting effects in the exchange, and develop mitigating strategies for the dilution. This experiment uses two doglegs with a deflecting mode cavity between them to exchange the horizontal and longitudinal emittances. This is followed by a short diagnostics section and a vertical spectrometer before the beam dump.

The 4x4 transverse/longitudinal transport matrix is of the form

$$R = \begin{pmatrix} A_{11} & A_{12} & B_{11} & B_{12} \\ A_{21} & A_{22} & B_{21} & B_{22} \\ C_{11} & C_{12} & D_{11} & D_{12} \\ C_{21} & C_{22} & D_{21} & D_{22} \end{pmatrix}.$$

Following the notation of D. Edwards [4], let α be the bend of each magnet in a dogleg and L_1 the distance between bends, then the dog leg matrix is given by

$$M_{dog} = \begin{pmatrix} 1 & L_1 & 0 & \alpha L_1 \\ 0 & 1 & 0 & 0 \\ 0 & \alpha L_1 & 1 & \alpha^2 L_1 \\ 0 & 0 & 0 & 1 \end{pmatrix} = \begin{pmatrix} 1 & D/\alpha & 0 & D \\ 0 & 1 & 0 & 0 \\ 0 & D & 1 & \alpha D \\ 0 & 0 & 0 & 1 \end{pmatrix}$$

where D is the dispersion. Let this be followed by a drift, L_2, to a thin lens deflection mode cavity. The cavity matrix is given by

$$M_{cav} = \begin{pmatrix} 1 & 0 & 0 & 0 \\ 0 & 1 & T & 0 \\ 0 & 0 & 1 & 0 \\ T & 0 & 0 & 1 \end{pmatrix}.$$

Where for exchange $T = -1/D = \dfrac{-1}{\alpha L_1} = \dfrac{\omega}{c}\dfrac{eV_{cav}}{E_{beam}}$ and V_{cav} is the deflection strength of the cavity and E_{beam} is the beam energy.

The total exchange is

$$M_{dog}L_2M_{cav}L_2M_{dog} = \begin{pmatrix} 0 & 0 & -\frac{1}{\alpha}-\frac{L_2}{D} & -L_2\alpha \\ 0 & 0 & \frac{-1}{D} & -\alpha \\ -\alpha & -\alpha L_2 & 0 & 0 \\ \frac{-1}{D} & \frac{-1}{\alpha}-\frac{L_2}{D} & 0 & 0 \end{pmatrix}.$$

In our geometry D=0.33 m and $\alpha = 22.5°$.

For a finite length cavity, the (4,3) element of M_{cav} enters and the on-diagonal (coupling) blocks start to show nonzero values and will dilute the 2D emittances, especially the smaller one. The finite length cavity also causes the equilibrium orbit to follow a staircase trajectory through the cavity. These effects can be compensated to some extent by suitable choices of beam and cavity parameters.

The A0PI experiment attempts to exchange a 6 mm-rad normalized transverse emittance with a 120 mm-rad (204 keV-ps) normalized longitudinal emittance. The beamline was commissioned in the summer of 2007 and measurements of the transport matrix are underway. Preliminary data has been taken of the beam emittances before and after the exchange, and analysis of that data is ongoing and will be the Ph.D. thesis of Tim Koeth. (The layout of the current beamline is shown in Figure 6.1 in Appendix 6.2.)

After initial evidence that the emittance exchange was occurring, our experimental program has concentrated on measuring the 6-D emittance exchange transport matrix. Figure 2.1 shows preliminary results of the transport matrix measurements as a function of cavity strength T. The circles represent the data and the red lines are what is expected from the model. The agreement is quite good for 12 of the 16 elements. We believe the discrepancy in the remaining elements is due to errors in the model, in particular how the dipoles are handled.

These measurements have shown a need for improved diagnostics. In particular, we are preparing a Martin-Puplett interferometer for measuring sub-picosecond bunch lengths and larger OTR screens to image the resulting large transverse beam spot. Additionally we have begun to measure the synchrotron and coherent synchrotron radiation that is a consequence of the beam parameters and beamline geometry.

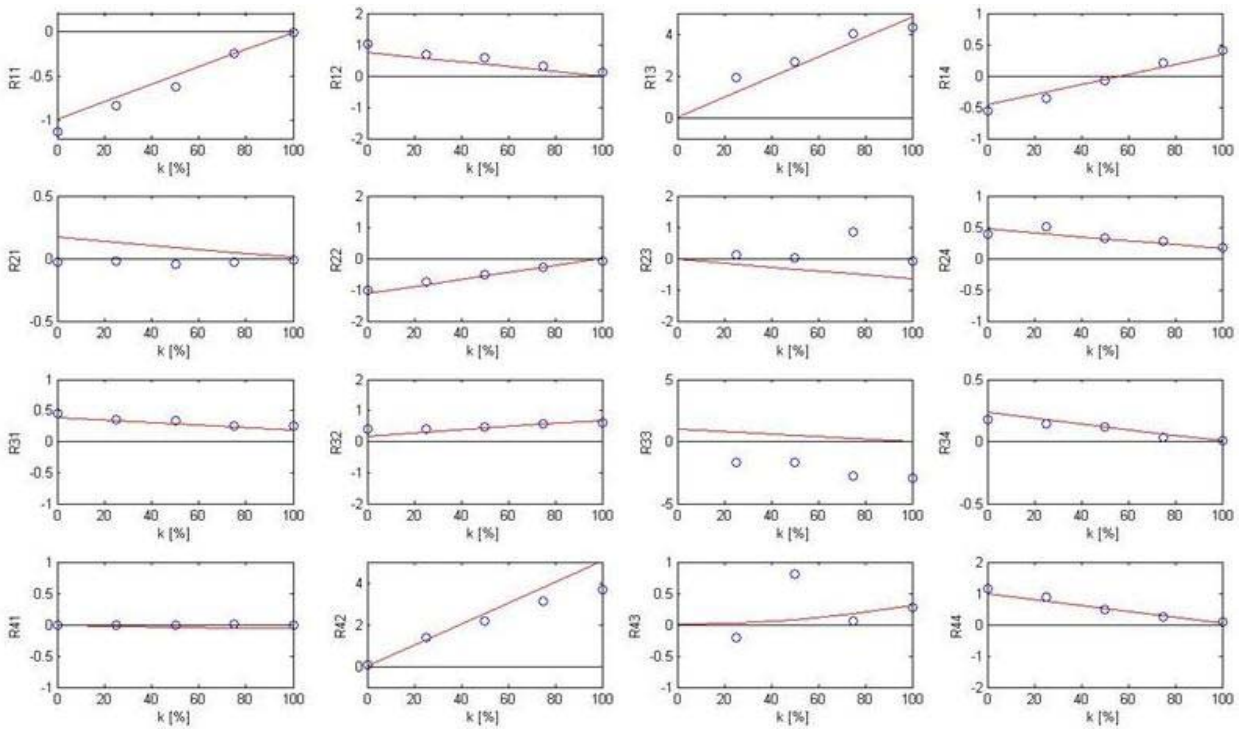

Figure 2.1: The transport matrix as a function of k (= T in the text). The circles are the measurements. The red lines are derived from the ELEGANT model.

We are proposing to continue and expand this experiment with the following program.

Step 1: Measure the emittance exchange

The transverse emittances are measured with a multislit screen which gives a complete picture of the transverse phase space ellipse. The longitudinal emittance measurements are currently limited to separate energy spread and bunch length measurements which provide an upper bound on the longitudinal emittance. Energy spread is measured with a beam screen after a spectrometer, and the bunch length is measured using a streak camera for bunches longer than 1 ps, and a Martin-Puplett interferometer for bunches shorter than 1 ps. Currently the instrumentation is not configured to measure the energy-time correlation of the bunch either at the input or the output of the exchanger. However, it may be possible to transport the light from the screen after the spectrometer to the streak camera, which would give us the energy-time correlation.

These measurements will be done at the low charge of 100 pC/bunch to reduce effects of space charge (SC) and coherent synchrotron radiation (CSR). These two effects increase the beam emittance and distort the phase space. This will require longer bunch trains to increase the signal/noise from the available diagnostics – in particular the bunch length measurements. A deflecting mode cavity would be advantageous for these measurements since a YAG screen could be used to image the beam with single bunches and achieve a higher resolution than can be obtained with the interferometer or streak camera.

Step 2: Measure a reversed exchange

Most suggested applications of the emittance exchange require exchanging a small longitudinal emittance with a large transverse emittance. The experiment proposed in Section 2.2 of this proposal will use a femtosecond laser to produce an ellipsoidal beam. Such a laser can produce a beam with a normalized transverse emittance of 1 mm-mrad and 5 mm-mrad longitudinal emittance with 200 pC of charge. By detuning the emittance compensation in the gun, it will be possible to detune the transverse emittance to 10 mm-mrad [5]. This beam can then be used to do the more interesting exchange of a small longitudinal emittance with a large transverse emittance.

Step 3: Manipulate the input phase space ellipse to tune the output phase space ellipse

Tuning the input transverse phase space ellipse will modify the output longitudinal phase space ellipse and vice versa. We can tune the beam for short bunches, or low momentum spread, by adjusting the spot size prior to the exchange. Adjusting the input energy chirp of the beam will adjust the output transverse phase space ellipse. The reason to study the effect of the input phase space ellipses is to look for different output conditions like shorter bunches and for the effects of non-zero elements in the A and D blocks of the transport matrix due to the finite length cavity. These elements will lead to coupling of the emittances and increase the measured emittances after the exchange. This effect is most dramatic in the longitudinal emittance after the exchange since it is the smaller of the two. These measurements will be done at the low charge of 100 pC/bunch to reduce effects of SC and CSR, which increase the beam emittance and distort the phase space.

Step 4: Arbitrary tailoring of the current distribution of a relativistic electron bunch.

Very recently a scheme to arbitrarily shape the current profile of an electron beam was proposed [6]. The technique relies on the emittance exchanger in the following way. An incoming beam is first transversely shaped upstream of the exchanger; then the emittance exchanger maps the transverse profile into the time profile thereby resulting in a tailored time distribution. Tailoring the longitudinal profile of an electron beam has tremendous applications ranging from super-radiant operation of a free-electron laser (by using a beam consisting of microbunches) to several advanced accelerator concepts. Linearly ramped bunches are known to increase the transformer ratio in beam-driven acceleration techniques (such as dielectric and plasma wakefield acceleration). Preliminary calculations indicate the possibility to generate bunch trains with 80 fs spacing at 15 MeV (see Figure 2.2). At the A0PI the generation of sub-picosecond bunch trains could be directly observed downstream of the emittance exchanger by a suitable choice of slits parameters. The main diagnostics would be a sensitive THz detector to measure the coherent transition radiation produced by such a train of bunches.

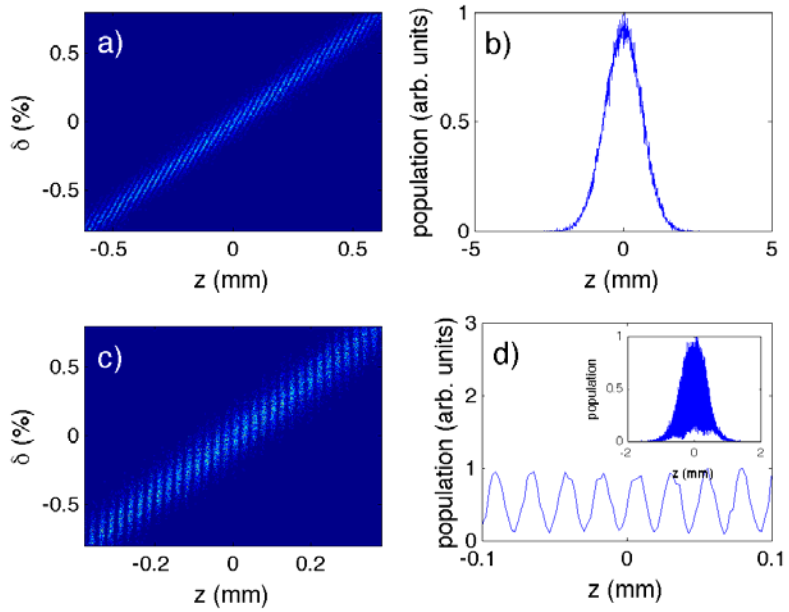

Figure 2.2: Simulation of pulse train generation using a transverse-to-longitudinal emittance exchanger. Zoomed longitudinal phase space (a) and corresponding longitudinal projection (b) downstream of the exchanger. Zoomed longitudinal phase space (c) and associated projection (d) downstream of a small magnetic chicane (R56=0.03 m). The beam upstream of the exchanger was passed through a series of horizontal slits with 0.1 mm width and 0.2 mm spacing (edge-to-edge). The inset in plot (d) correspond to the profile over the full bunch extent while the main plot is a zoom for -0.1 < z (mm) < 0.1.

2.2 Generation of ellipsoidal bunches from Cs_2Te cathodes

Thee-dimensional ellipsoidal charge distributions produce linear space charge fields within the distribution and are in principle free of space-charge-induced phase space dilution. Schemes to generate such a distribution using a photo-emission electron source were proposed by Serafini [7] and more recently by Luiten, *et al*. [8]. In the proposed method a short laser impinges a prompt photo-emitter. The operating parameters of the electron source are chosen such that the distribution evolution is dominated by the linear space charge force. This space-charge-dominated expansion can be achieved provided

$$\frac{eE_0 c\tau_l}{mc^2} << \frac{\sigma_0}{\varepsilon_0 E_0} << 1,$$

where E_0, τ_l are respectively the peak electric field on the photocathode and the time duration of the photoemission process, and $\sigma_0 \approx Q/(\pi r^2)$ is the charge density (Q the bunch charge and r the radius of the laser on the photocathode). For a prompt photocathode τ_l is comparable to the laser pulse duration. Using the A0PI nominal operating parameters E_0=35 MV/m, for charge Q~0.1 pC and assuming a laser pulse length τ_l = 50 fs we have $eE_0 c\tau_l/(mc^2) \approx 0.001$ and $\sigma_0/(\varepsilon_0 E_0) \approx 0.1$ so the condition for ellipsoidal bunch generation can in principle be achieved. However, this requires a photocathode drive laser capable of producing a ~50 fs laser pulse, e.g. a Ti:Sapphire oscillator and regenerative amplifier. The generation of ellipsoidal bunches from

magnesium [9] and copper [10] cathodes was recently demonstrated, however generating such a distribution out of a high quantum efficiency semiconductor cathode such as Cs_2Te would be an important proof-of-principle experiment. Several projects based on such cathodes rely on, or would benefit from, ellipsoidal bunches [11]. Using the A0PI as a test bed for such an experiment would present significant improvements and complement the recent experiments performed at UCLA and TU-Eindhoven.

Besides generating ellipsoidal bunches, the A0PI also incorporates an accelerating cavity which could be used to further accelerate and/or manipulate the bunch. For instance the cavity could be used to remove the large correlated energy spread thereby providing insight on the origin of slice energy spread. Furthermore the first dogleg used in the emittance exchange experiment could be modified to be achromatic and would therefore act as a bunch compressor enabling the generation of ~kA peak current.

Preliminary simulations of the generation and transport of ellipsoidal bunches at the A0PI were performed using the particle tracking code ASTRA. An example of distributions at z=3.77 m from the cathode (downstream of the accelerating cavity) are presented in Figure 2.3. For these simulations the charge is 50 pC and all the accelerator settings are identical to the ones presently achieved at the A0PI (the current A0PI setup is used for these simulations). The simulation supports the generation of ellipsoidal bunches as inferred from the (z,x) configuration space. The normalized transverse emittance obtained in these simulations is 0.8 μm (this number includes the thermal emittance using an excess kinetic energy of 0.55 eV at the photocathode). Thorough numerical optimization of the ellipsoidal production and transport scheme still remain to be done.

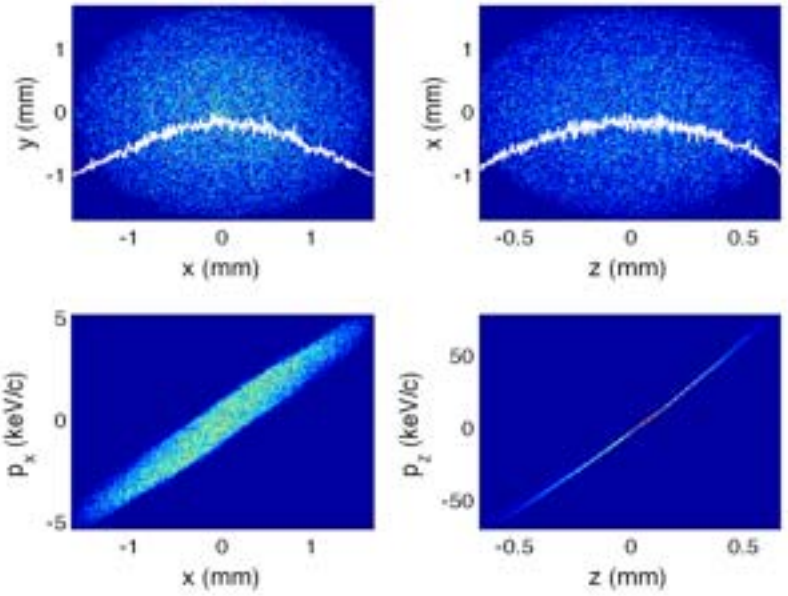

Figure 2.3: Transverse (top right), side (top left) configuration spaces and transverse and longitudinal phase spaces at z=3.77 m obtained by impinging a 50 fs (rms) laser on a Cs_2Te cathode. The simulations are for Q=50 pC and all parameters except laser pulse length are similar to the ones presently achieved at the A0PI.

We have also peformed a simulation of a possible bunch length and time distribution diagnostic using the currently used 5-cell 3.9 GHz copper cavity. The setup includes a set of quadrupoles, the deflecting cavity and a YaG screen 1.2 m downstream (Figure 2.4). The quadrupoles are used to focus the beam on the YaG screen when the cavity is off. When the cavity is turned on the ellipsoidal character of the distribution can be inferred (see Figure 2.5), e.g., from the top right picture (which is representative of the (*z,y*) distribution) along with the associated (parabolic) distribution.

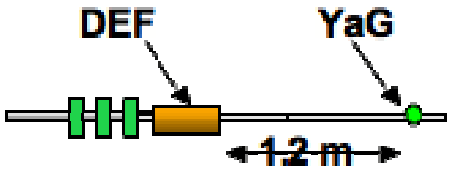

Figure 2.4: Experimental setup to measure the time distribution of the 15 MeV ellipsoidal bunch using the current copper deflecting cavity.

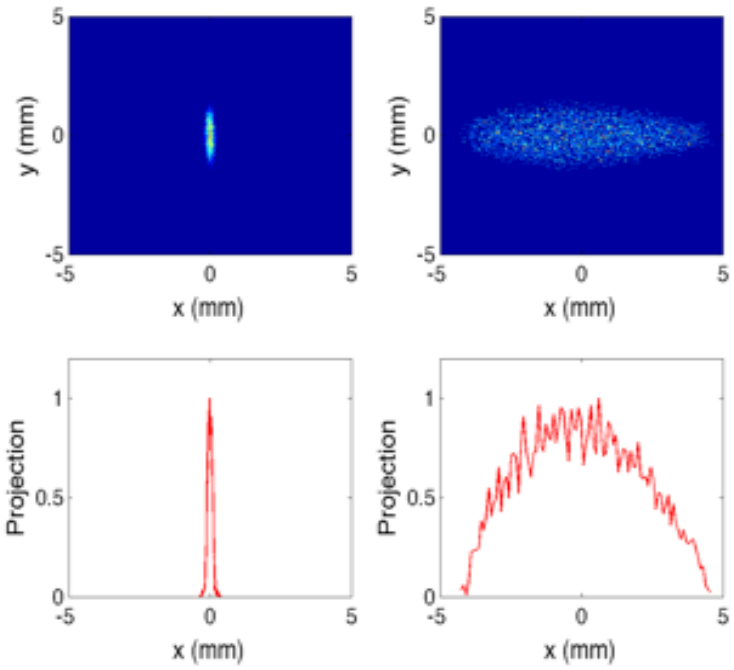

Figure 2.5: Simulation of bunch length measurement using the present copper deflecting cavity. The top images are the beam spots downstream of the cavity on a YaG screen, the bottom plot are the corresponding projection along the horizontal axis (the cavity is horizontally deflecting the beam). The right and left columns respectively correspond to cavity on and off.

2.3 Other experiments under consideration

2.3.1 Round-to-flat beam transformation and image charge undulator

High intensity x-rays can be generated from large synchrotron radiation or FEL facilities using electron beams at GeV energies. The image charge undulator (ICU) [12][13] offers an opportunity to generate high intensity x-rays using electron beams of much lower energy generated by a much more compact and less expensive electron source. With sub-millimeter gratings, the radiation produced by an ICU can be in the hard x-ray regime for an electron beam energy less than 200 MeV. Currently, there has not been an experimental demonstration of the image charge undulator. At the A0PI we have the experience of producing flat electron beams with emittance ratio 100:1 [14] with normalized rms beam emittance of 0.4 and 40 μm. This experience provides an advantage to pursue a proof-of-principle image charge undulator experiment using planar gratings.

An ICU will require a flat electron beam with a transverse emittance smaller than what has been achieved in round-to-flat beam transformation experiments to date. This program provides additional motivation for extending those experiments.

As shown in Figure 2.6, the ICU consists of two identical metal gratings on either side of the beam vacuum. The electron beam induces its image charge on the metal gratings which apply a Lorentz force (wake field) on the electron beam. Due to the periodic geometry of the gratings, the image charge wake field alternates just like in a conventional magnetic undulator. This process leads to the undulating motion of the electron beam.

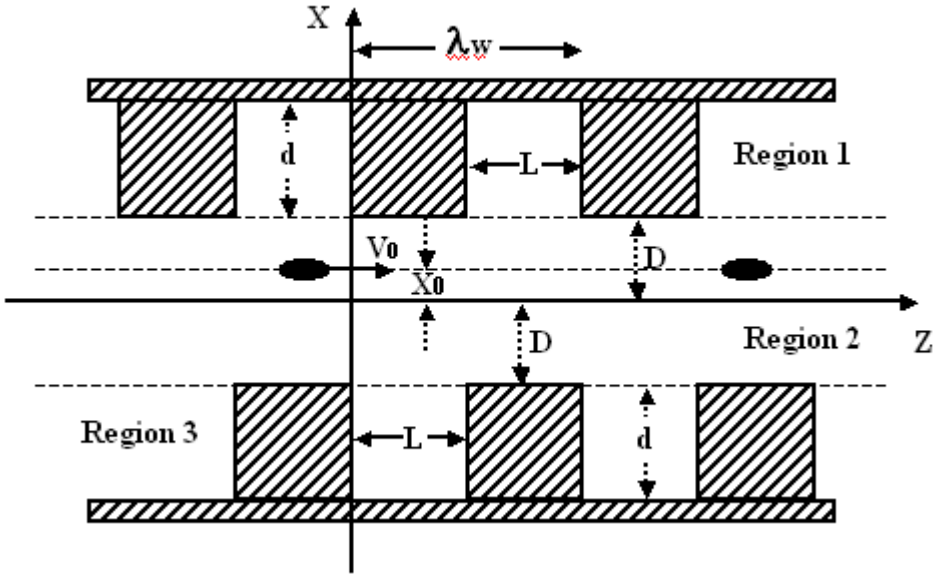

Figure 2.6: Schematic of a 2-D image charge undulator (from ref. [13]).

For a uniform sheet beam and infinitely long undulator, the magnetic field of the image charge wake field has only a non-alternating component which is parallel to the grating groove direction (i.e., B_y only). The vertical electric field near the undulator center is given by

$$E_x(z) = E_0 \sum_{n=1}^{\infty} N_{2n+1} \sin(2n+1)k_w z, \quad E_0 = \frac{\sigma}{2\varepsilon_0},$$

where σ is the surface charge density of the sheet beam, ε_0 is the permittivity of free space, and $k_w=2\pi/\lambda_w$ is the wave number. The dimensionless coefficients N_{2n+1} depend only on the geometry of the image charge undulator and are given by

$$N_{2n+1} = -\frac{a_n \tanh(2n+1)\pi\frac{d}{L}}{(n+\frac{1}{2})\pi \sinh(2n+1)\pi\frac{D}{L}}.$$

The strength of the transverse electric field is determined by the electron beam charge and size (E_0), as well as the grating geometry (N_{2n+1}). As d approaches 0 (no grating) the image charge force vanishes, and as D decreases the image charge force becomes larger. Keeping only the first term of the transverse electric field, the equation of motion in the vertical direction is

$$v_x(z) \approx \frac{cK}{\gamma}\cos(k_w z); \qquad K = \frac{eE_0 N_1}{mc^2 k_w}.$$

where v_x is the vertical particle velocity. The radiation mechanism follows as in a magnetic undulator, so one may borrow the formulae for the radiation wavelength, spectral and angular distribution of the photons, etc. For example, the radiation wavelength is given by

$$\lambda = \frac{\lambda_w}{2\gamma^2}\left(1+\frac{K^2}{2}\right).$$

For a bunch charge of 1 nC, beam (hardedge) thickness, width, and length of 10 μm, 150 μm, 100 μm, respectively, undulator period of 50 μm, and D/L = 0.5, d/L = 1, the image charge undulator parameter K is about $1.06\text{x}10^{-2}$. The photon angular density of nth harmonic in the central cone N_p^n (in units of photons per second per mrad per 0.1% bandwidth) is given by [15]

$$\left.\frac{dN_p{}^n}{d\Omega d(\Delta\omega/\omega)}\right|_{\theta=0} = 1.74\times10^{14} N_g{}^2 E_e{}^2[\text{GeV}] I[\text{A}] F_n(K).$$

where N_g is the number of grating period, E_e the beam energy, I the current, and $F_n(K)$ is given by

$$F_n(K) = \frac{K^2 n^2}{(1+K^2/2)}\left\{J_{\frac{n-1}{2}}[\frac{nK^2}{4(1+K^2/2)}] - J_{\frac{n+1}{2}}[\frac{nK^2}{4(1+K^2/2)}]\right\}^2$$

Integrating the angular density over the solid angle, we have the number of the photons per second per 0.1% bandwidth given by

$$\frac{dN_p{}^n}{d(\Delta\omega/\omega)} = 1.34\times10^{14} N_g Q_n I(A), \text{ where } Q_n(K) = (1+K^2/2)F_n(K)/n.$$

The bandwidth near the nth harmonic is given by

$$\frac{\Delta\omega}{\omega} = \frac{2.8}{n\pi N_g}.$$

Now consider the first harmonic of the radiation. For an electron beam energy of 30 MeV, a bunch train of 1 nC separated by 1 μs (current = 1 mA), $F_1(K)$ = 1.1 x10^{-4}, a 3.4 cm long ICU will produce 8x10^9 photons per second per mrad per 0.1% bandwidth in the central cone at 7.3 nm radiation wavelength, which is about 1x10^{10} photons per second per 0.1% bandwidth integrated over the solid angle. The bandwidth is about 0.1%.

The ICU will require a flat electron beam of suitably small emittance. Over the grating length of 3.4 cm, the beam thickness cannot exceed 2•D, which corresponds to a maximum divergence of about 0.3 mrad. Given a thickness of 10 μm at the ICU center (waist), this corresponds to a normalized emittance of about 0.05 μm for a $\beta_0 \sim 1$ cm. This is ~1/8 of the normalized emittance achieved in round-to-flat beam transformation experiments to date, which were performed at half the charge proposed here. This set of numerical calculations is listed in the "Soft-X" column in Table 2.1, as well as other numerical examples of undulator, beam and photon parameters.

Table 2.1: Numerical examples of the image charge undulator experiment parameters

		Green	far UV	Soft-X
Grating tooth width (L)	μm	500	250	25
Grating tooth depth (d)	μm	500	250	25
Grating separation (2D)	μm	500	250	25
Grating period	μm	1000	500	50
Bunch charge	nC	1	1	1
Beam energy	MeV	16	30	30
Beam length	μm	1000	500	100
Beam width	μm	500	250	150
Beam thickness	μm	100	50	10
Radiation wavelength	nm	510.01	72.54	7.25
Undulator parameter K		6.33e-3	1.27e-2	1.06e-2
Gain length	cm	47.91	22.46	3.40
Grating period in a gain length		479	449	679
Norm. rms vertical emittance	μm	0.40	0.40	0.05
Norm. rms horizontal emittance	μm	3.53	3.53	8.42
Norm. rms round beam emittance	μm	1.19	1.19	0.65
emittance ratio		9	9	170

There are several upgrades that can improve the performance of the round-to-flat beam transformation [16]. This includes the upgrade of the RF gun to one with an axial symmetric coupler – which reduces the degradation of the flat beam transformation from the gun asymmetry. More importantly, if the upgraded RF gun can be operated at higher gradient, this will help mitigate the space charge force, which is the major degrading factor in the round-to-flat

beam transformation. With an additional acceleration cavity the beam energy can be increased to ~50 MeV. Apart from further reducing the space charge force, this upgrade will also make it possible to obtain higher photon energy and larger photon flux. Furthermore, if the flat beam can be compressed through a magnetic bunch compressor, the higher peak current can give rise to a larger image charge force, which will enhance the image charge undulator strength. In this case, the addition of a new dipole mode cavity will provide an improved bunch length measurement.

The numerical example for an ICU given here is a 2-D model with an infinitely long sheet electron beam. In fact, the beam transverse and longitudinal distributions will influence the process. There are other theoretical models [17] that treat an axially symmetric wake field undulator that can be adapted to study our planar case.

Contrary to the conventional undulator, the wiggling strength in an ICU is not uniform. The beam has a finite emittance and a certain longitudinal distribution, which will influence the radiation process. Numerical simulations need to be performed to understand how these factors will affect the radiation process. Furthermore, there will be other types of significant longitudinal and transverse wakes such as those induced by the Smith-Purcell process. We will identify a proper simulation tool to study these issues.

Experimentally, due to the very small gap between the two gratings, it will be a technical challenge to send the beam through the ICU. One of the first things one can explore is to simply arrange two pieces of flat metal surfaces without any gratings on them, and try to gain some experiences by transporting the electron beam through the small opening between these simple metal surfaces [18].

2.3.2 Ring beam generation

The generation of ring beams has several potential applications in beam physics. First, ring beams can be used in beam-driven collinear acceleration such as dielectric wakefield based on a cylindrical symmetric structure [19][20]. In this scheme a high charge drive hollow beam excites the wakefield in the dielectric structure and a probe beam propagating on the structure axis is accelerated. In the past, such attempts at low energy resulted in an instability that prevented the scheme from properly working. Therefore the generation and transport of high charge hollow beams is an interesting topic that could be pursued at the A0PI.

On the other hand such ring beams, if properly manipulated, might result in very bright beams since for the same charge, a ring beam has a lower charge density than its counterpart uniform cylindrical beam. We therefore conjecture that the transverse phase space dilution due to space charge would be mitigated and if a proper transformation capable of converting this hollow beam into a uniform beam would be implemented at high energies, the final beam could have higher brightness than otherwise achievable. A possible manipulation consists of producing a magnetized ring beam (by immersing the cathode in an axial magnetic field) and using the round-to-flat beam transform to create a beam with a hollowed transverse phase space in one degree of freedom. A method to coalesce this hollow phase space into a single-peaked phase space distribution was first suggested by Derbenev [21], and one implementation was recently worked out [22][23]. The scheme as envisioned today requires a lengthy focusing channel or a small isochronous ring to perform the transformation, but with further design study could be pursued as a possible future addition to the A0PI or NML facility.

2.3.3 Microbunching Diagnostics and Experiments

Over recent years there has been considerable study of possible microbunching processes in linacs that provide short bunches with high peak current for FEL application. These linacs have magnetic bunch compression that can convert energy modulation to charge density modulation after the compressor. High frequency components in the beam can result from coherent synchrotron radiation (CSR), wakefields, and longitudinal space charge (LSC) effects. In particular, modulations in bunch charge can provide energy modulation through space charge that can then be amplified in the compressor resulting in further charge modulation at higher frequency due to compression. Such an effect was initially hinted by start-to-end simulation of LCLS and a theory was developed in Reference [24]. Because of the possibility of this effect, the XFEL has incorporated a "laser heater" to be able to increase the uncorrelated energy spread.

This beam microbunching has caused unexpected enhancements of the beam images from optical transition radiation (OTR) beam profiling screens. This has been observed at LCLS [25], APS [26], and FLASH. The ultra low emittance beams at a small focus exceed the threshold for YAG:Ce scintillator linearity, so OTR screens are indicated. However, following bunch compression there seems to be a combination of LSC and CSR induced microbunching that results in these coherent OTR (COTR) emissions nonuniformly fluctuating over the beam image. The LCLS is presently precluded from using their OTR screens from 135 MeV to 14.3 GeV to perform reliable beam profile and hence emittance measurements. Besides the diagnostics complication there may be a contribution to the emittance degradation in the chicane bends from COSR and FIR CTR. Examples of the data taken at APS at 150 MeV in collaboration with staff there are shown in Figure 2.7 where the almost 10 times more intense spikes show up near maximum compression in the image and profile at the right.

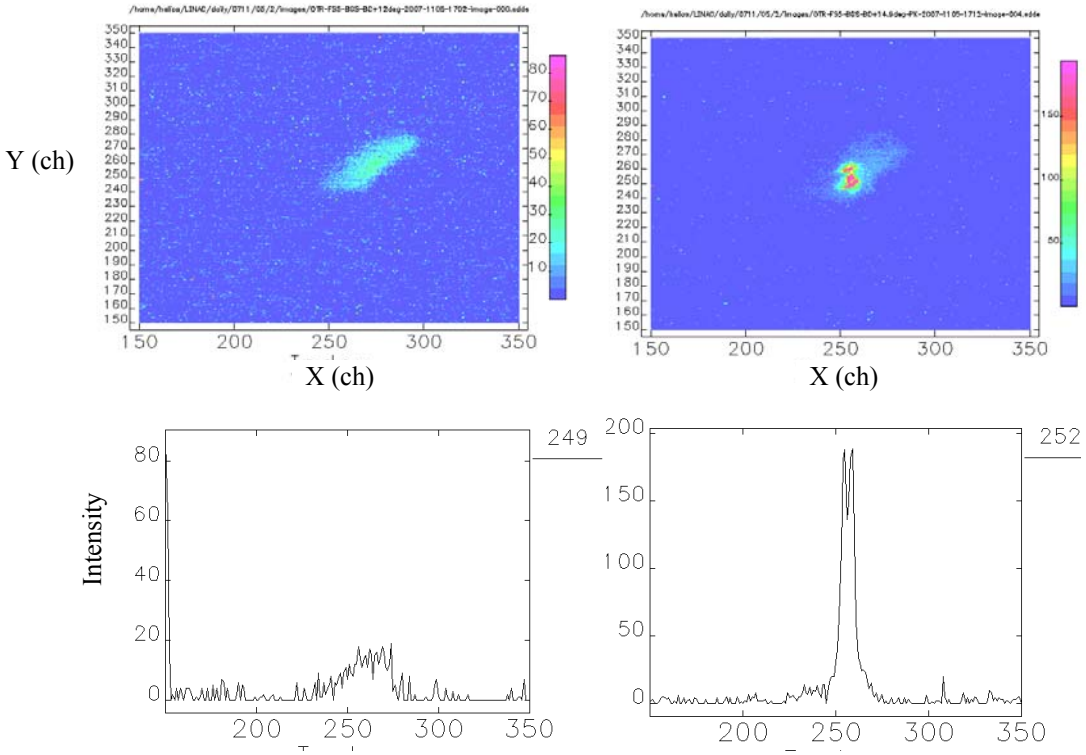

Figure 2.7: Comparison of the OTR images obtained after the chicane at low compression (top left) and high compression (top right). The corresponding x profiles through the images are shown in the two lower plots. The enhancement is about a factor of ten in the profile on the right.

What seems to surprise people is that this coherent effect shows up in optical frequencies, and there is speculation as to the generation mechanism [27]. It is not known if these fundamental LSC effects will be evident at 15 - 50 MeV following bunch compression of the bunches to sub-500 fs FWHM bunch lengths. There is speculation by J. Rosenzweig that freezing space charge is important and that we may not be at high enough energy. However, there is known to be a strong charge dependence of LSC so the use of 4-6 nC per bunch rather than 0.5 nC could compensate for the lower energy. There is also the possibility of looking in the near IR where the effects could be larger. Currently, we only compress in the dogleg configuration at A0, and we have not yet seen the effect in our brief inspections of the beam images. We plan to reinstall a compressor in the straight ahead line that will make possible observation easier. Initial measurements and modeling would look for the effect and how to possibly generate it by inducing bunch modulation. We suspect that the emittance exchange experiment at A0 will also be an interesting test on the microbunching effect. It is possible that the x-z exchange would mitigate the effect. If the effect can be observed, further studies and modeling of it and its mitigation would be warranted. The understanding and mitigation of this effect has become a critical task for LCLS, Elettra, and other advanced accelerators. It has been one topic of this year's Zeuthen CHBB Workshop in May 2008, and there is now a second Microbunching Instability Workshop devoted to this topic planned at LBNL in October 2008. The A0PI and NML facilities could be used to uniquely explore high charge and lower energy parameter space in the USA and also uniquely compare the results of bunch compression by a chicane and by EEX. If a LSC instability effect is found at 3 nC per micropulse at γ=60, we could then consider

the option of a laser heater operating on the third harmonic of the resonant wavelength to mitigate the effect at A0 and NML.

References

[1] Y. Orlov *et al.*, CLNS Report 91/1092 (1991); CBN Report 91-9 (1991).

[2] M. Cornacchia, P. Emma, Phys. Rev. ST Accel. Beams **5**, 084001 (2002).

[3] K.-J. Kim, A. Sessler, in *AIP conference Proceedings **821***, p 115.

[4] D. Edwards, *Note on transit in deflecting mode pillbox cavity*, WWW Document, (http://nicadd.niu.edu/aard/emittance_exchange/dae20aug20.pdf).

[5] P. Piot, private communication.

[6] P. Piot, Y.-E. Sun, M. Rihaoui, in *Proc. 13th Advanced Accelerator Concepts Workshop, Santa Cruz, CA* (2008, to be published).

[7] L. Serafini, in *AIP Conference Proceedings **413***, p. 132 (1997).

[8] J. Luiten, *et al.*, Phys. Rev. Let. **93** (2004).

[9] P. Musumeci, *et al.*, Phys. Rev. Let. **100** (2008).

[10] J. Luiten, *et al.*, in *Proc. 13th Advanced Accelerator Concepts Workshop, Santa Cruz, CA* (2008, to be published).

[11] R. Legg, *et al.*, in *Proc. EPAC2008, Genova, Italy*; W. Graves, private communication.

[12] Y. Zhang *et al*., in *Proc. FEL2002, Argonne, IL*.

[13] Y. Zhang *et al.*, in *Proc. PAC2003, Portland, OR*, p. 941.

[14] P. Piot *et al.*, Phys. Rev. ST Accel. Beams **9**, 031001 (2006).

[15] K.-J. Kim, Eq. (4.44) in practical units, in *AIP Conference Proceedings **184***, p. 600.

[16] Y.-E. Sun *et al.*, in *Proc. PAC2005, Knoxville, TN*, p. 3774.

[17] A. Opanasenko, in *Proc. EPAC2004, Lucerne, Switzerland*, p. 2415.

[18] A. Zholents, A0PI Review Committee discussions, Fermilab (August 18, 2008).

[19] P. Shutt, in *Proc. All-union Conference on New Methods of Charged Particle Acceleration*, (Springer, NY 1989).

[20] J. L. Hirshfield, in *Proc. 13th Advanced Accelerator Concepts Workshop, Santa Cruz, CA* (2008, to be published).

[21] Y. Derbenev, NIM A **441**, 223 (2000).

[22] S. Nagaitsev, Mathcad simulation program, private communication (July 2008).

[23] D. Edwards, M. Syphers, "Comments on an Experiment on Transverse Coalescing" (unpublished).

[24] E. Saldin *et al*., TESLA-FEL Report 2003-02 (2003).

[25] R. Akre *et al.*, Phys. Rev. ST Accel. Beams **11**, 030703 (2008).

[26] A.H. Lumpkin, *et al*., "Observation of Enhanced OTR Signals from a Compressed Electron Beam", in *Proc. BIW2008, Lake Tahoe, CA* (to be published).

[27] J. Rosenzweig, in *Proc. 13th Advanced Accelerator Concepts Workshop, Santa Cruz, CA* (2008, to be published).

3 Advanced beam instrumentation

Besides the measurement of fundamental beam parameters (intensity, position, transverse size and emittance), the experiments proposed at the A0PI require advanced instrumentation to observe in detail the longitudinal characteristics of the bunches. The requirements will be even more stringent when shorter bunches are generated with the Ti:Sapphire laser and EEX. Therefore most of the proposed plans for advanced beam instrumentation focus on longitudinal beam parameter characterization: bunch length, bunch profile, and bunch time-of-arrival. Each of the presented methods has its particular strengths and weaknesses; none is able to fully characterize the complete range of longitudinal bunch parameters adequately in a single shot, non-invasive manner. The instrumentation capabilities are summarized in Table 3.1.

Table 3.1: Bunch length measurement devices with the applicable ranges and features of each.

Device	**Applicable Bunch Lengths**	**Comments**
Deflecting Mode Cavity	100 fs – 2 ps	well understood; expensive; measure single or a few bunches (warm cavity) or many bunches (cold cavity)
Streak Camera	> 1-2 ps to 40 ps	well understood; expensive; measures single bunch; commercial device; dispersion effects dominate short bunch measurements; provides arrival times and jitter
Martin-Puplett Interferometer	< few ps	slow response; scanned over many macropulses; susceptible to upstream CSR and wakefields; missing phase makes details of bunch profile difficult to obtain
CTR angular distribution	< few ps	parametric measurement of bunch profile; must input assumed shape; scanned over many macropulses; susceptible to upstream CSR and wakefields
Electro-optical Sampling	100 fs – 2 ps	single shot measurement; expensive; must understand behavior of electro-optical crystal in frequency regime corresponding to expected bunch lengths; usceptible to upstream CSR and wakefields (less so than CTR and M-P Int.)
Waveguide Pickup	200 fs – 2 ps	inexpensive and simple, but absolute calibration is very difficult; does not give shape, just rough bunch length

3.1 Deflecting mode cavity

Deflecting mode cavities provide a method of measuring the longitudinal bunch distribution and have been used for many years at SLAC and DESY for this purpose[1][2]. The method relies on the transverse kick as a function of beam arrival time in the deflecting cavity. This kick maps the bunch length into the deflecting plane. If the beam is imaged at a suitable location downstream of the deflecting cavity then the longitudinal bunch profile can be determined. If this device is coupled with a spectrometer magnet bending in the other plane, then a complete picture of longitudinal phase space may be obtained.

At the A0PI a streak camera is currently used to measure bunch lengths, and it has a single bunch resolution of ~1.5 ps rms. At bunch lengths shorter than 1 ps, a Martin-Puplett interferometer is used, but this method requires multiple bunches per train and many minutes of data taking to obtain an accurate measurement. The analysis relies on certain assumptions of the bunch shape and frequency response of the detector in order to reconstruct the shape of the bunch and also loses information about the head-tail orientation of the bunch.

We wish to improve our method of measuring short bunch lengths by using a superconducting deflecting mode cavity operating at 3.9 GHz. Extensive design work has already been committed to such a cavity, and much of the technology and design will be based on 3.9 GHz acceleration mode superconducting cavities being built by FNAL for DESY. In addition, a 3.9 GHz acceleration mode cavity will be required at NML for generating very short bunches. Our goal for a deflecting mode cavity is to have a system that can measure the bunch length of a single bunch with a resolution ~50 fs rms over a large range of bunch lengths, at a beam energy up to 50 MeV which will be available at NML.

Currently at the A0PI there is a 3.9 GHz 5-cell normal-conducting copper cavity based on a superconducting deflecting cavity design for a separated kaon beam experiment. This cavity is cooled with liquid nitrogen to increase the Q and separate the modes. It is powered by an 80 kW klystron, and the integrated deflecting field is 550 kV. It is currently used for the emittance exchange experiment at the A0PI. It does not have sufficient voltage for measuring bunch length with the required accuracy at 50 MeV beam energy. A superconducting cavity constructed with 9 cells will provide approximately 2.5 MV integrated deflecting field.

Figure 3.1 shows the beamline with a matching section prior to the cavity, the deflecting cavity, a drift length and a flag to image the beam. The purpose of the matching section is to focus the beam at the flag when the cavity is turned off. We shall assume that the beam can be focused to a 0.1 mm rms spot at the flag, and the flag has a pixel resolution of 28 μm.

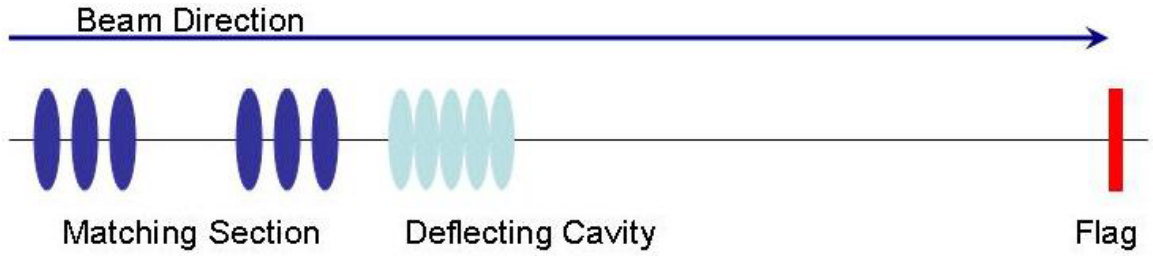

Figure 3.1: Schematic drawing of a bunch length measurement using a deflecting cavity.

The deflecting cavity is operated at the zero crossing of the deflecting field which will give no net deflection to the bunch, and kick the head and tail in opposite directions. The beam spot at the flag, with the deflecting cavity on, is then

$$\sigma_{x-flag}^2 = \sigma_{x-cavoff}^2 + \sigma_z^2 k^2 \left(L + \frac{L_c}{2}\right)^2$$

where $\sigma_{x\text{-flag}}$ is the beam spot at the flag location, $\sigma_{x\text{-cavoff}}$ is the beam spot at the flag when the cavity is turned off, σ_z is the bunch length at the deflecting cavity, L_c is the deflecting cavity length, and L is the drift length from the downstream end of the cavity to the flag. k is given by

$$k = \frac{eV\omega}{Ec},$$

where eV is the integrated transverse kick, c is the speed of light, ω is the angular frequency and beam energy is E. For the 9-cell superconducting cavity, k=4.1 m^{-1} at 50 MeV, and, for comparison, the 5-cell copper cavity currently in use at the A0PI has k=0.9 m^{-1} at 50 MeV. To measure a 100 fs bunch with a resolution of 50 fs will require a lever arm (L) of only 0.9m using a 9-cell superconducting cavity. For comparison, the 5-cell normal conducting cavity will require a lever arm of 4.8 m.

Over the years considerable development work has been done on the design of a deflecting mode cavity. Prototypes have been built and a 3-cell cavity tested in a vertical dewar. It achieved 7.5 MeV/m deflecting gradient (Figure 3.2).

At the A0PI all the cavity ancillaries will use the designs developed for the 3.9 GHz accelerating mode "3rd harmonic cavities". These include input coupler, HOM coupler designs, helium vessel, and tuner. Outstanding design issues are associated with the lower order mode (LOM) and other polarization mode damping. These will be the real R&D developments for this design and are related to future applications such as crab cavities for the ILC interaction region. For the application at the A0PI we will be running short bunch trains and mode damping will not be that much of an issue. Even so, this is an opportunity to try various LOM designs.

The cryogen insulating vacuum module will be designed to accommodate one 9-cell cavity of either accelerating or deflecting variety. It will interface to the standard cryogen feed "top hat" design used both at the A0PI and in the Meson Lab SRF test areas. The length and diameter of the vessel will be ~ 1.1 m and 0.5 m, respectively.

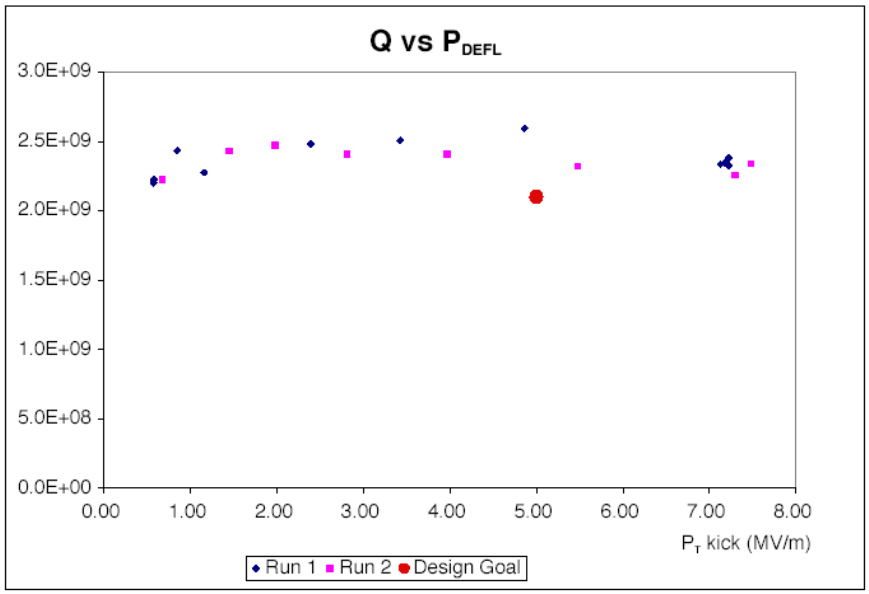

Figure 3.2: Results from a 3-cell TM110 deflecting mode cavity. Large red dot is design value; pink and blue dots are measurements. 7.5 MV/m corresponds to 120 mT maximum surface field.

3.2 Electro-optical sampling

Electro-optical (EO) sampling has been proven to be a very effective non-intercepting technique for measuring longitudinal bunch information [3]. We propose that EO sampling be studied with the present A0PI and integrated into the upgraded A0PI. The goals of EO sampling at the A0PI are to develop methods not explored at other accelerators and to provide a fully operational diagnostic tool for other A0PI experiments. Presently, the unique EO sampling opportunities at the A0PI are: (1) measure longitudinal bunch information of low energy electron beams; (2) measure longitudinal bunch distribution for bunch lengths up to a few ps; and (3) investigate the use of alternate laser wavelengths via fiber lasers. As cross-checks, longitudinal bunch information from EO sampling will be compared with streak camera measurements (see section 3.3.1), Martin-Puplett interferometer measurements (see section 3.3.2), and with the future deflecting mode cavity (see section 3.1).

Currently, most single–shot EO sampling experiments are carried out using spectral decoding, temporal decoding, or spatial decoding [4]. Each technique has unique properties that must be evaluated in terms of the bunch measurement requirements. Among the three methods, temporal decoding is able to measure the shortest bunches, spatial decoding has been used as a fs resolution clock at advanced light sources [5], and spectral decoding has been effective in measuring longer pulses.

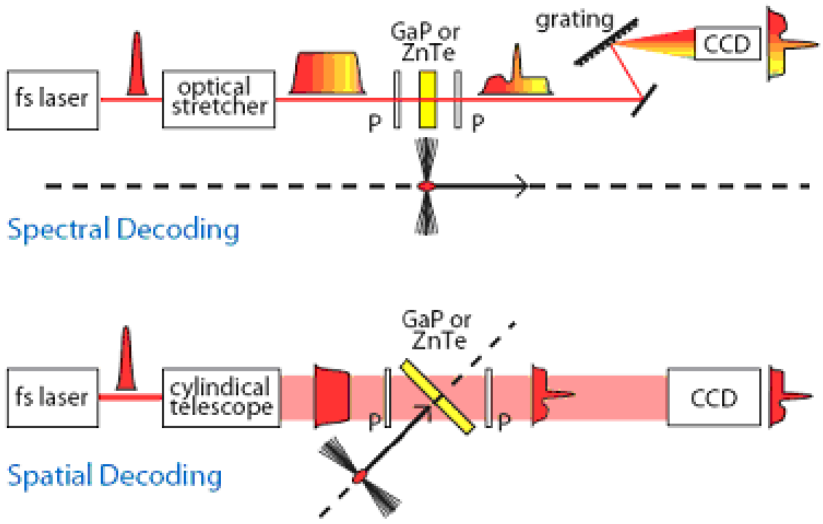

Figure3.3: Schematic representations of the 3 common single shot EO detection techniques for investigation at A0PI [4].

Our efforts and plans at the A0PI will concentrate on developing single-shot EO sampling based on the spectral decoding and spatial decoding techniques to investigate low energy electron beams with bunch lengths 200 to 2000 fs (rms). Figure 3.3 shows schematics of both spectral and spatial decoding methods. In addition, current EO studies are focused on high energy beams (few hundred MeV and higher). EO sampling of low energy electron beams has not been studied, and our proposed research will address this low energy gap.

We will also concentrate on developing a suitable fiber laser system for EO sampling. Present EO sampling methods utilize expensive Ti:Sapphire lasers. In addition, transport of the Ti:Sapphire beam to the beamline is problematic. Fiber lasers may solve these problems and make EO methods more convenient and affordable for multiple locations in a large accelerator facility.

Current A0PI Laser System

The bandwidth of our current Nd:YAG laser system is too small to do an optimal EO experiment, however, this laser can still be used to begin our EO sampling efforts. Because of the longer bunches and limited bandwidth of the Nd:YAG laser, it will difficult to chirp the laser pulses enough to perform spectral decoding, therefore we will do an initial experiment with spatial decoding using the current laser system on long bunches up to a few ps. We expect to accomplish two things in this experiment. First we will learn more detail of the uncompressed A0PI electron beam longitudinal structure and compare it to our streak camera measurement. Second we will have in place a suitable optical path and EO beamline device for a future fs laser system (Ti-sapphire or fiber laser).

Ti:Sapphire laser system

A Ti:Sapphire laser is used to generate ultrashort pulses (down to 10's of fs) because of its large bandwidth. To date most EO experiments have used commercial Ti:Sapphire systems, and we also plan to use a commercial system. We have formed a collaboration with Argonne National Laboratory (ANL) and Northern Illinois University (NIU) to study EO sampling

Because of the availability of an amplified Ti:Sapphire laser at ANL, initial EO experiments have been carried out at the Advanced Wakefield Accelerator at ANL. At ANL we have already used a ps laser pulse to focus on a ZnTe crystal to generate terahertz radiation as measured with a LN_2-cooled Golay cell. In the next stage, an EO setup with a spatial decoding technique will be assembled using parts already purchased. After this stage the setup will be moved into the AWA beamline and experiments with beam will be carried out.

At NIU, a new Ti:Sapphire and amplifying system has been purchased. One graduate student has been assigned to carry out bench-top studies in the NIU laboratory. After these bench-top measurements, the laser setup will be moved to the A0PI and experiments with the electron beam will be conducted. Both spectral and spatial decoding will be investigated. This work will be a major component of the student's Ph.D. thesis project. In addition, advanced EO studies, such as real-time beam structure and position monitoring, will be carried out using this setup.

Fiber laser system

Although a Ti:Sapphire laser system is the laser of choice in current EO studies, it is expensive and difficult to distribute to several accelerator positions. A fiber laser of appropriate wavelength and power will alleviate these difficulties.

There are two approaches we are pursuing. First, we will use an Er-doped fiber laser (1530 nm) which has already been purchased for time-of-arrival EOM measurements (see section 3.1.3), to investigate both spectral and spatial decoding techniques. One difficulty with this approach is that the group velocity mismatch inside the commonly used EO crystal (such as ZnTe or GaP) between the THz wave and 1530 nm is larger than the Ti:Sapphire case. This is a severe problem for measurements of very short bunches (<200 fs). This will not be an issue in our measurements of 200-2000 fs bunches. At the same time we will also investigate the possibility of using frequency doubling of the 1530 nm as our EO probe. Second we will construct in-house a fs fiber laser based on Yb-doped fiber (1030 nm). This wavelength would greatly reduce the mismatch caused by the longer wavelength Erbium laser. Figure 3.4 is a simulation of EO sampling for different laser wavelengths and shows that the change in measured bunch length is small for a 1 ps bunch. This indicates that EO sampling with fiber lasers is a viable option for the intermediate bunch lengths proposed at the A0PI.

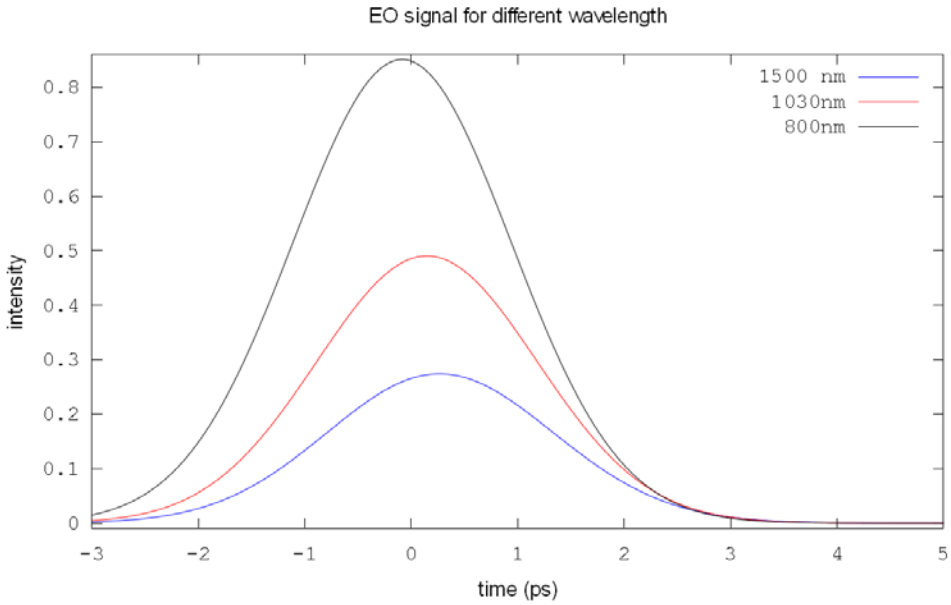

Figure 3.4: Simulated EO signal using 3 different laser wavelengths. Electron beam bunch length is 1 ps rms with a bunch charge of 1 nC. The EO sampling crystal is 1 mm thick ZnTe and 5 mm away from the beam center. Gaussian fits of these curves give rms values of 1.025 ps, 1.032 ps and 1.06 ps for 800 nm, 1030 nm and 1500nm respectively.

3.3 Other instrumentation development

3.3.1 Streak camera

The opportunity for a new series of streak camera experiments at the A0PI was recognized in the last year. The enabling upgrade was adding the synchroscan option to the existing C5680 Hamamatsu streak camera mainframe. By locking this module to the 81.25 MHz subharmonic of the RF system, the synchronous summing of bunches could be done with a trigger jitter of <1.5 ps (FWHM) for both the UV drive laser harmonic and the e-beam via optical transition radiation (OTR). This summing allowed the needed bandpass filters to be utilized to reduce the chromatic temporal dispersion effects inherent to the use of the broadband OTR source and the transmissive optics components. In addition, the C6768 delay module with phase feedback was also acquired, and this stabilized the streak camera sweep relative to the master oscillator so that the camera phase drift was reduced to the picosecond level over tens of minutes. This latter feature allowed a series of experiments to be done on the bandwidth effects and transit time effects in the respective transport lines, including evaluation of the matrix elements of the emittance exchange line.

In the course of our experiments, we have done a series of tests on the chromatic temporal dispersion effects for this particular input optics barrel with UV transmitting optics and our optical transport lines. Our effects are less than that reported at SSRL with optical synchrotron radiation and their transport [6], but ours still needed to be characterized carefully to allow accurate bunch length measurements using the OTR. We now use a 550-nm longpass filter as a compromise on effective bandwidth and the reduced variation in group velocity with wavelength in the red end of the spectrum. This results in a contribution to system time resolution of about

2.6 ps (FWHM) due to this bandwidth effect including a quartz window, one quartz lens, and the input optics barrel. The optics barrel lens set is the largest contributor. The intrinsic tube resolution for a single wavelength is 1.5 ps FWHM (0.6 ps σ). At the shortest bunch lengths the sensitivity to changes becomes reduced as one works near the system resolution value.

After characterizing the UV laser bunch length, a series of e-beam experiments on the A0PI beamlines was performed [7]. We have measured a significant bunch length elongation versus bunch charge for the present conditions in the uncompressed line and showed that this is consistent with ASTRA calculations. We also observed a time-dependent transverse focusing effect at 4 nC/bunch as shown in Figure 3.5. Such a "self-pinching" effect is observed in typical high charge bunch simulations. Our experiments indicate the bunch head and tail to have 50% larger transverse size than the bunch central slices. The bunch length is 28 ps (FWHM). This topic merits further study in FY09. Detailed beam dynamics simulations using particle-in-cell calculation will be performed and the evolution of the (x,t) configuration pattern will be studied for different electron source settings (solenoids, and laser (flat top versus Gaussian distribution)

One of our more critical measurements this year was the verification of the x-z emittance exchange process by graphically showing the reduction in the bunch length when the 5-cell cavity is at 100% power compared to power off. This is shown in Figure 3.6 where the horizontal axis is in seconds, or shot number, for each state of the cavity power, and the vertical axis is the corrected bunch length. The FWHM length reduction from 5.2 ± 0.7 ps to 1.4 ± 0.9 ps is clear. Note however that the 1.4 ps number is below the resolution band width limit so its absolute value includes some systematic error.

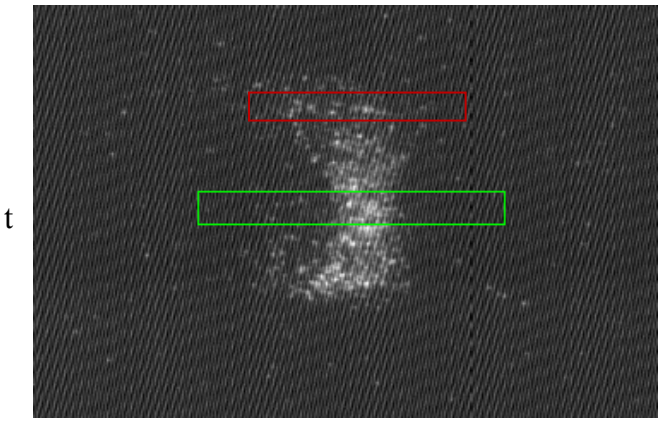

Figure 3.5: Evidence of time-dependent transverse focusing effects in a 4-nC bunch.

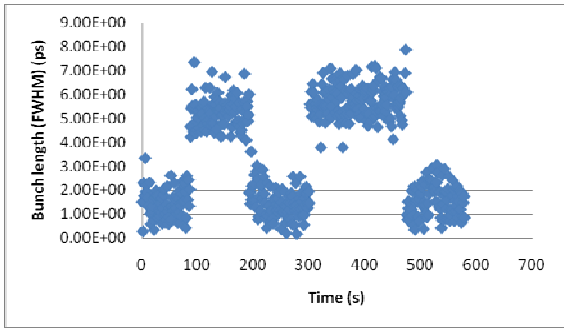

Figure 3.6: Direct measurement of the x-z emittance exchange and the bunch-length reduction with the 5-cell cavity power on versus 5-cell cavity power off.

Plans

We have just started our dual-sweep streak camera experiments to look for phase jitter and slew within the laser and e-beam bunches. We expect to continue our efforts to reduce the chromatic temporal dispersion effects by testing a grating pair as a compensator or by acquiring a commercial mirror-input-optics assembly for the camera. If either is successfully employed, we

can reduce the effective system resolution limit by a factor of ~2 and be able to use 4 times more bandwidth of broadband OTR to improve image statistics. We are also evaluating purchase of a new 12-bit digital readout camera for the streak camera. The combination of these features will bring us closer to single-`bunch longitudinal profile measurements at the 1 nC level at A0PI upgrade energies and will enable slice-emittance tests. This system would support any future x-z emittance exchange experiments, laser/e-beam relative phase tests, and bunch compression tests in FY09 and later. We also could support qualification of the Martin-Puplett interferometer and the CTR angular distribution bunch length measurement methods that are just underway or planned.

The optical transport line will be redesigned to increase OTR signal collection efficiency and allow us to observe the drive laser in the same streak image with the OTR. The direct relative phase information (peak centroid positions) should be obtainable at the 300 fs level or one camera system pixel. With dual-sweep mode, we should be able to investigate sub-bunch transients and accelerator phase feedback loop issues.

The streak camera system is currently used routinely for beam characterizations and in the x-z emittance exchange experiments. With the proposed upgrades, it can continue to be the reference longitudinal profile and phase measurement device at the 1-2 ps level. It can be used in the development and commissioning of the other techniques that will push measurement capabilities further towards the 100-300 fs level.

3.3.2 Martin-Puplett interferometer

One method for determining the bunch length of an electron beam is autocorrelation interferometry. Interferometric bunch length measurements are possible because of the relationship between the magnitude of the spatial spectrum of the bunch and the spectral content of Coherent Transition Radiation (CTR) from the bunch. Since the spectrum of CTR is a function of only the magnitude of the bunch spectrum (no phase dependence), an exact determination of the longitudinal charge distribution cannot generally be obtained. However, for certain simple shapes, such as Gaussians, the approximations necessary to obtain phase information do a fairly good job of preserving the main parameters of the bunch, such as width.

At the A0PI we have installed a Martin-Puplett interferometer [8], borrowed from DESY (Fig. 3.7). A Martin-Puplett interferometer is a polarizing type interferometer which in this case uses closely spaced wire grids for the polarizers and splitters. The grids consist of 15 μm diameter gold-plated tungsten wires spaced by 45 μm.

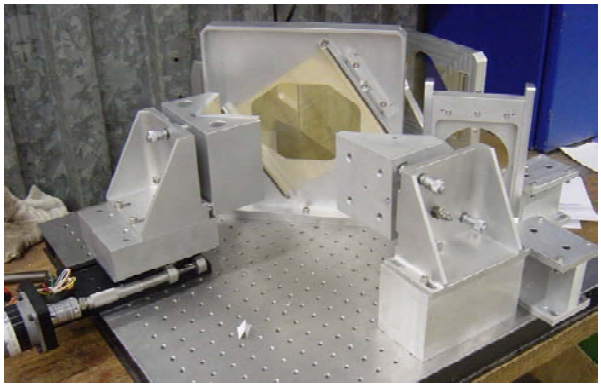

Figure 3.7: Photograph of the interferometer. The gold-colored portion is the wire grid beam splitter.

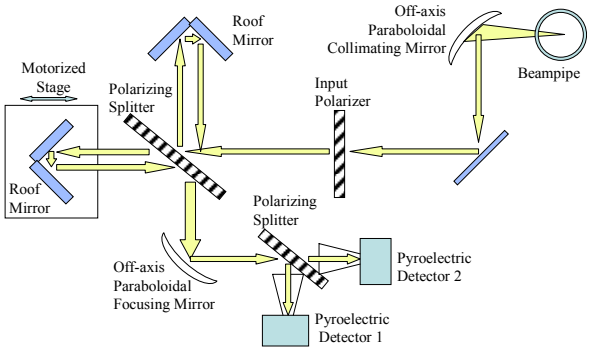

Figure 3.8: Schematic of the interferometer.

The CTR exits the beamline through a quartz window and is immediately collimated by a 200 mm focal length off-axis parabolic mirror (Fig. 3.8) to prevent loss of light through the interferometer.

A complication in this technique is the fact that due to the small size of the CTR screen (1.25 cm radius), there is a strong diffraction effect which in turn introduces a frequency-dependence (broadening) of the angular distribution. The extent of this broadening depends on $\gamma\lambda$. Combined with a finite aperture, this leads to a reduction in long wavelengths in the interferogram. We have a plan to replace the existing radiator with a simpler shape to facilitate correcting the interferogram.

Another issue with this system is the lack of knowledge of the spectral response of the detectors and possible interference effects. We are currently testing a broadband Schottky diode detector as a possible replacement for the pyroelectric detectors and plan to have the pyroelectric detector spectrum measured.

Comparison of Streak Camera and M-P Interferometer Results

Initial comparisons of the Martin–Puplett Interferometer with the streak camera were made on 6/18/08 (Figure 3.9). The streak camera data used a 40 bunch synchronous sum, and the interferometer scans were done over tens of minutes. The data involved the power cycling of the 5-cell cavity which, because of the x-z exchange, compresses the bunch length, but increases the horizontal transverse beam size and divergence. This change in the horizontal emittance may have an impact on the measurement. The ratio of 5-cell on/off measurements was 0.66 for the bunch length from the streak camera, 0.69 for the interferometer autocorrelation peak width, and 0.43 for the reconstructed interferometer bunch lengths.

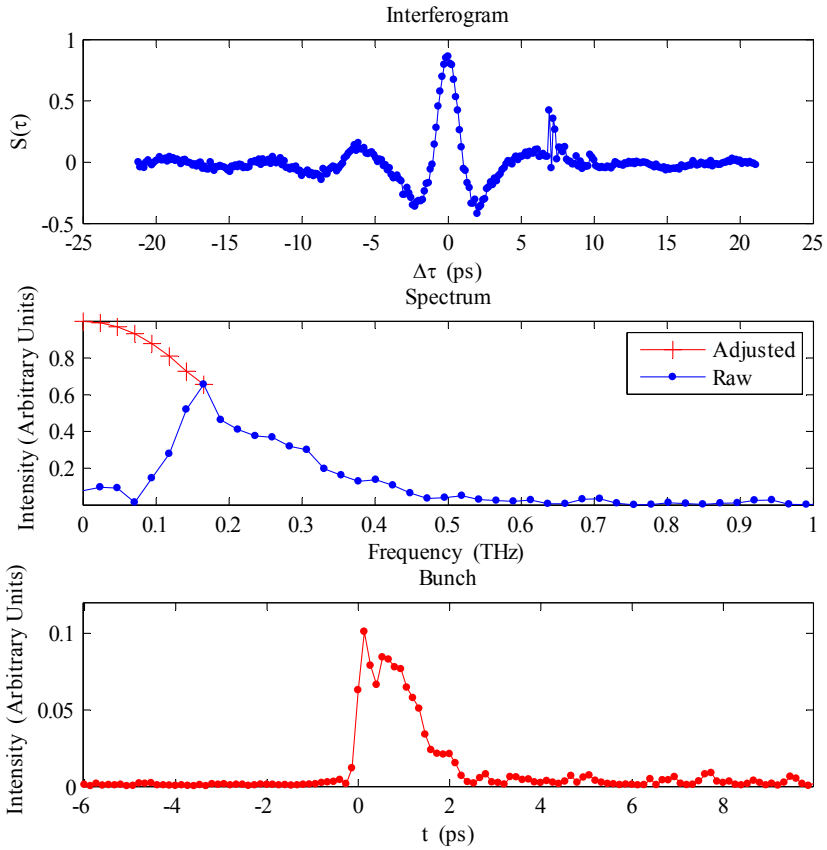

Figure 3.9: Autocorrelation trace (top), raw spectrum (middle blue), corrected spectrum (middle red), and reconstructed bunch (bottom) from 5-cell on/off data.

Plans for the Future

We plan to replicate this interferometer since it is borrowed from DESY. We also plan to replace the existing radiator with a simpler shape to facilitate correcting the interferogram for diffractive effects. Another issue with the current system is the lack of knowledge of the spectral response and possible interference effects in the pyroelectric detectors. We are currently testing a broadband Schottky diode detector and a golay cell as possible replacements for the pyroelectric detectors and we also plan to have the pyroelectric detector spectrum measured.

3.3.3 Electro-optical modulator for time-of-flight measurement

The stability of accelerators depends on the synchronization between the beam, low-level RF, and other accelerator components. A precise measure of the bunch time-of-arrival (TOA) with respect to the master oscillator clock signal is important. Operation of future accelerators places a requirement of measuring the bunch TOA to an accuracy of better than $1/10^{th}$ of a degree of the RF. This results in a need to measure TOA at a resolution better than a few 100 fs. Precision measurement experiments at the A0PI require bunch TOA measurements to the same resolution.

A bunch TOA monitor with a few 100 fs resolution is in development at the A0PI and is based on a system developed at DESY [9]. The monitor is based on conversion of time to voltage for amplitude modulation of a pulsed laser via Electro-Optical Modulation (EOM). Figure 3.10

shows the basic principle of the bunch TOA monitor. The zero-crossing voltage of a broadband beam pickup is used to amplitude modulate a single 100 fs wide laser pulse. Figure 3.11 shows how the zero-crossing voltage changes as a function of the bunch arrival time.

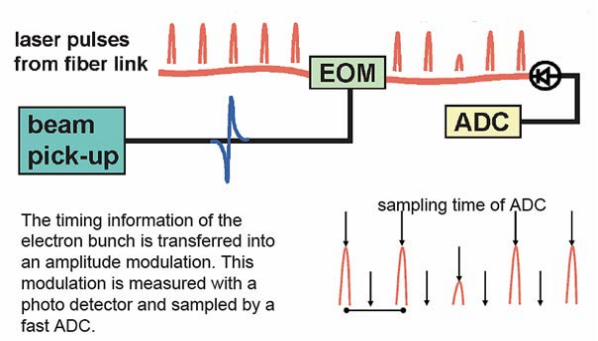

Figure 3.10: Basic principal of the bunch time-of-arrival monitor

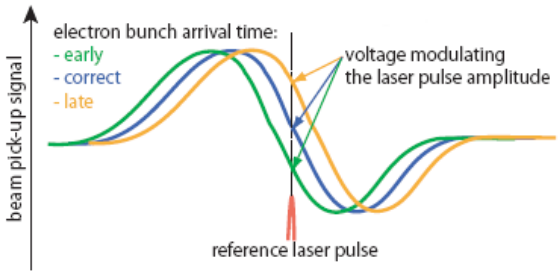

Figure 3.11: Relation between the modulation voltage signal to the bunch arrival time.

Figure 3.12 shows a block diagram of the A0PI TOA monitor. A wide bandwidth beam pickup, needed to permit femtosecond TOA measurements, acquires the bunch electric field. Using a precision variable delay line, the pickup signal is timed to arrive at the electro-optical modulator in coincidence with the laser pulse. The zero-crossing of the RF signal is used to modulate the amplitude of a 100 fs wide laser pulse. The photodiode converts the laser pulse into a voltage which is sampled by an ADC.

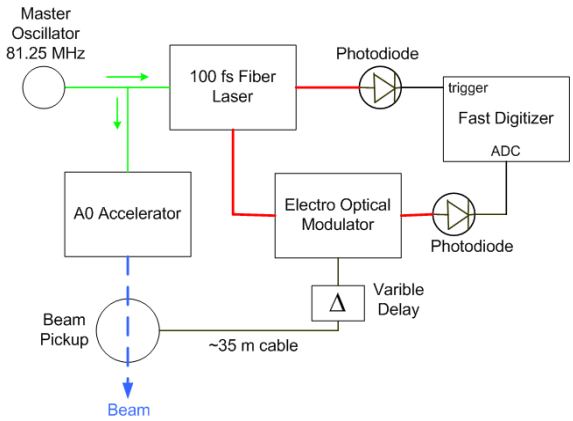

Figure 3.12: Schematic of the TOA at the A0PI.

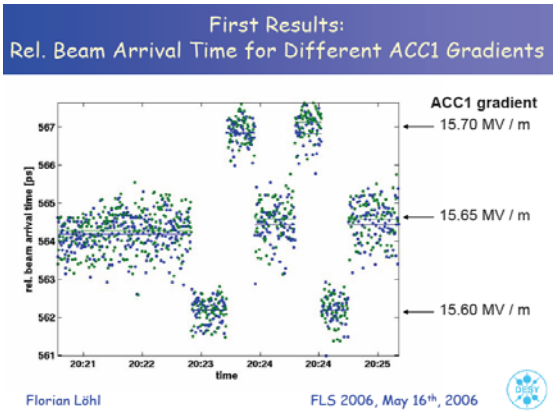

Figure 3.13: First results from DESY FLASH: time-of-arrival vs. accelerating gradient.

A similar monitor has been developed at DESY as a sub-100 fs bunch arrival monitor for the FEL accelerators. Figure 3.13 show the first results from the DESY bunch arrival monitor [10]. These initial results illustrate the potential resolution ability of an EOM bunch time-of-arrival monitor at the A0PI.

3.3.4 Optical transition radiation interferometry

The use of optical transition radiation interferometry (OTRI) to determine the rms beam divergence of electron beams is a well-established technique for electron linac applications [11]. The technique uses imaging-at-infinity optics to obtain the angular distribution of the OTR. In this case an interference pattern is generated by electrons passing through two thin foils separated by a distance comparable to $\gamma^2\lambda$, where γ is the Lorentz factor and λ is the wavelength of the OTR. The photon phase difference from the two sources determines the interference pattern which contains information about energy and angular spread or divergence in the beam at the given λ. The energy of the beam and the foil separation determine the angular width of the fringes. At lower gamma, the multiple scattering of the electrons in the first foil is one of the issues for measuring an actual beam divergence of less than 2 mrad (σ). Also at low gamma the foil spacing is typically sub-mm so one must image the OTR through the first foil. The scattering term, the actual beam divergence, and the imaging system effective resolution term can be treated as a quadrature sum to obtain the observed divergence value. In FY08 the techniques were developed for having the thin-foil planes normal to the beam rather than at 45 degrees to the beam to reduce the effective first-foil thickness by 0.707. This configuration involved imaging the OTRI pattern from a back angle. In addition the MCP was lens coupled instead of fiber-optically coupled to the CCD to improve the imaging angular resolution. This layout and optical scheme are shown schematically in Fig. 3.14. In this geometry the first foil also must be transparent to visible light. By choosing a 2.5-µm thick Mylar film for the first foil, the basic criteria are met of low scattering and visible-light transparency. As can be seen in Fig. 3.15, the modulation of the fringes is different experimentally and calculationally for the total beam divergences of 1.8 and 3.3 mrad. The data and the calculation are in good agreement except at the inner edge of the first fringe for each case.

In the context of the key x-z emittance exchange experiments at A0PI in FY09-10, such an OTRI setup will be used to verify directly the larger x divergence of 3-4 mrad expected after the exchange has occurred. At the same time it would show the vertical divergence unchanged (although limited in sensitivity by the first-foil scattering term). A linear polarizer will also be used to cleanly access the theta-x and theta-y axes of the angular distribution pattern.

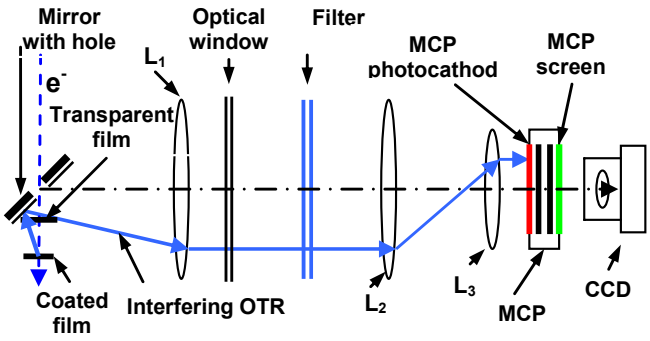

Figure 3.14: The OTRI setup with normal incidence of the electron beam.

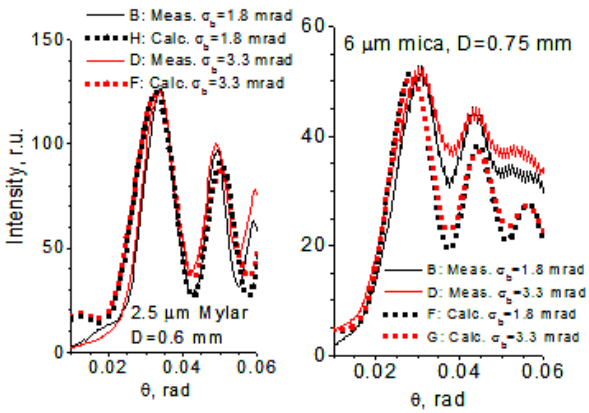

Figure 3.15: Measured (solid lines) and simulated (dotted lines) for a Mylar-based interferometer at normal incidence.

3.3.5 Longitudinal diagnostics via coherent radiation angular distribution

Coherent transition radiation (TR) and diffractive radiation (DR) spectra have been used to measure bunch lengths of picosecond electron bunches. However the angular distribution of this radiation also contains information on the longitudinal distribution of the bunch. When the size of the radiator, r, satisfies the condition $\lambda \sim 2\pi r/\gamma$ and radiation wavelength, λ, is on the order of the bunch length then the angular distribution of the radiation is very sensitive to the longitudinal distribution of the bunch [12]. Therefore by properly choosing the size of the radiator, for a given beam operating point, one can use the shape of the TR or DR angular distribution pattern to determine longitudinal information.

A flat screen radiator experiment has been proposed by Ralph Fiorito (University of Maryland) for the A0PI for making such angular distribution measurements. Theoretical models show that a well-defined radiator size allows for a bunch length measurement based on the angular distribution of the coherent TR at the A0PI. The coherent TR angular distribution will be measured using a highly sensitive Golay cell and a Schottky diode and compared to other A0PI longitudinal detectors such as the streak camera (see section 3.1.1) and the Martin-Puplett interferometer (see section 3.1.2).

Figure 3.16 shows the calculated angular distribution of coherent TR, using a radiator optimized for current A0PI beam parameters, for two different bunch lengths. The simulation shows the clear effect on the angular distribution due to change in bunch length. As part of the A0PI upgrade, a radiator optimized for these parameters will be installed.

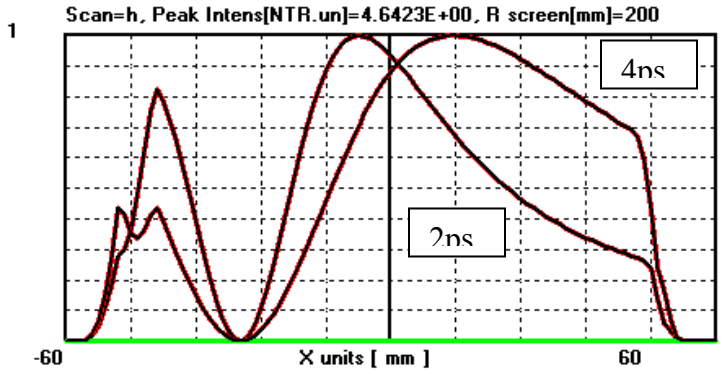

Figure 3.16: Calculated distribution of coherent TR observed from a flat detector plane at distance to source of 200 mm. The simulation is for 16 MeV electrons and Gaussian bunches of 2 and 4 ps width. The distribution is a horizontal scan from an optimized radiator size of 16 X 25 mm at 41 degrees to beam.

The advantages of this technique over other longitudinal measurements is that it is simple to experimentally implement, it can be performed at any transition radiation detector location and it can be tuned to measure sub-picosecond bunches. Presently, the measurements will be made with a scanning detector but an array of detectors could be developed to improve the time required for the measurement.

Measurements of the angular distribution of coherent TR and DR have been performed at the Swiss Light Source (SLS) at the end of the 100 MeV pre-injector [13]. Figure 3.17a shows the angular distribution of coherent TR with the theoretical best fit of a single Gaussian bunch shape

with a width of 0.69 ps. Figure 3.17b shows the same angular distribution but with a double Gaussian bunch shape fit. The best fit occurs for Gaussians widths of 0.57 and 2.84 ps with the second Gaussian shifted by 1.5 ps.

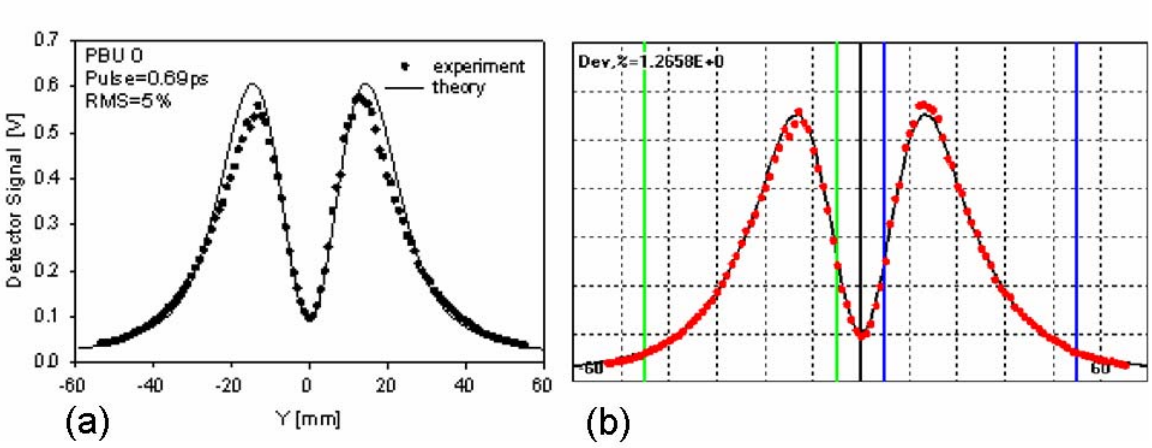

Figure 3.17: Measured coherent TR from 100 MeV electrons at SLS. (a) Theory curve is best fit model based on single Gaussian longitudinal bunch shape with a width of 0.69 ps. (b) Theory curve is best fit model based on double Gaussian longitudinal bunch shape with widths of 0.57 and 2.84 ps.

3.3.6 HOM signal processing

RF accelerating cavities can support, apart from the accelerating mode, a multitude of resonant modes, the so-called higher order modes (HOM). These modes are excited by the charged particle beams and can lead to an increase of the beam emittance or even to beam break-up in large accelerators. However, the HOMs can be useful for beam diagnostics [14,15]. The dipole modes have a linear dependency of their amplitude and phase with the beam offset and angle. Therefore they can be used for position monitoring, similarly to cavity beam position monitors (BPM). By measuring the phase of monopole modes excited by the beam with respect to the injected fundamental mode, one obtains the phase of the beam relative to the RF. The monopole and dipole modes are shown in Figure 3.18.

Broadband HOM-based beam phase detection

The HOM coupler, designed to absorb all higher order modes, except the fundamental acceleration RF is not perfect, thus some of the 1.3 GHz RF drive leaks through. This allows direct measurement of the beam excited phase of higher monopole modes with respect to the 1.3 GHz RF. A simple test system has been implemented in the FLASH linac at DESY which simply digitizes a single HOM coupler signal with a fast 20 GS/s, 5 GHz bandwidth scope and then uses Fourier analysis to measure the relative phase. This system has demonstrated a 0.1° (@ 1.3 GHz) measurement RMS over a couple of hours and has reproduced requested phase changes to the drive RF. In principle this measurement can be improved by implementing dedicated electronics to split the HOM signal and downmix the fundamental and a selected monopole to a convenient IF (~20 MHz) and then digitize. This should greatly improve the signal to noise but does introduce potential phase shifts which need to be understood. This

system is very useful to monitor the phase of the RF system and could be used to provide slow feedback for phase stability.

Narrowband HOM-based BPM and cavity alignment observation

The dipole modes behave exactly like a cavity BPM with very high Q. The system implemented at FLASH uses analog downmix electronics to downmix electronics shown in Figure 3.19 to select a dipole mode which couples strongly to the beam. Tests at FLASH have demonstrated resolutions of less than 10 μm for a single bunch and the ability to provide bunch-by-bunch measurements for 1 MHz bunch trains. The system requires calibration by moving the beam through known trajectories in the cavity which is typically done with other BPMs. The narrowband system is very timing sensitive and requires good stability between the RF, LO, and trigger.

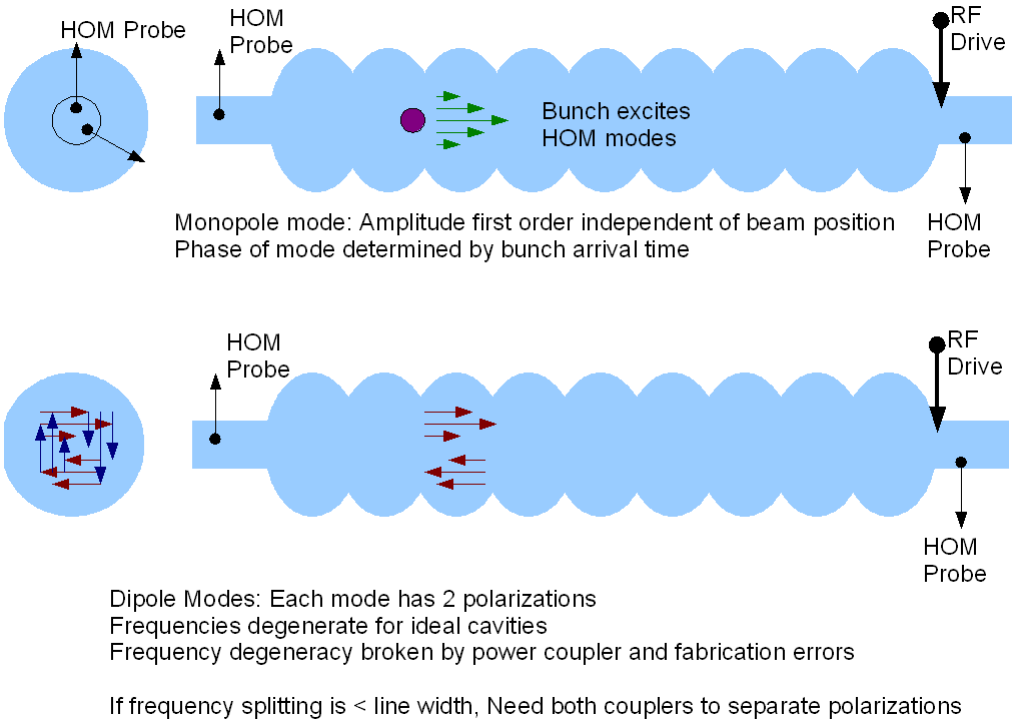

Figure 3.18: Monopole and dipole modes in a Tesla 9-cell cavity.

The HOM signals also are a very useful tool for studying the superconducting cavities under operating conditions. The observed modes can be compared to predicted modes from simulations and test stand measurements. For this reason, a narrowband system capable of measuring different modes is very attractive. This makes implementing the LO, trigger, and downmix electronics challenging given the phase stability which is required.

Plans

In the current A0PI accelerating cavity setup both HOM coupler signals are buried in the cryostat and are unfortunately not accessible. With a new or modified SCRF module these signals will be ported to the outside, allowing analysis of these HOM signals. We plan to investigate both techniques, broadband HOM signal analysis using our (to be upgraded) fast oscilloscope (12

GHz realtime BW), as well as a narrowband read-out system based on a 125 MSPS VME digitizer currently under development.

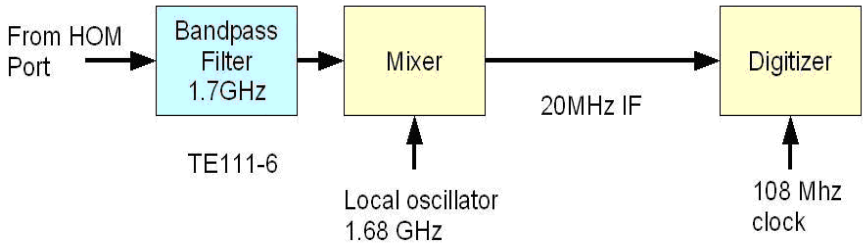

Figure 3.19: Narrowband downmix electronics scheme.

3.3.7 Cavity BPM

In frame of the ILC global design effort, a high resolution (0.5-1 μm) beam position monitor, based on a common-mode free L-Band cavity is under development for application in the SRF cryostat (quad-BPM package) (Figure 3.20) [16]. The manufacturing of a warm prototype is currently underway, it has dipole-mode read-out ports (f_{110}~1.5 GHz) for the displacement signals, as well as monopole-mode ports (f_{010}~1.1 GHz) for beam intensity normalization. The loaded Q is Q_l~500-700, which allows single bunch beam position measurements (>300 ns bunch-to-bunch spacing). After tuning and characterization on an RF test stand, we are planning to analyze the cavity BPM in detail under realistic beam conditions at the A0PI. It is necessary to understand how well the tuning suppresses the x-y coupling, CM rejection in the dipole mode signals, single bunch behavior, signal processing, noise figures, etc. to fully characterize resolution and dynamic range under real world conditions.

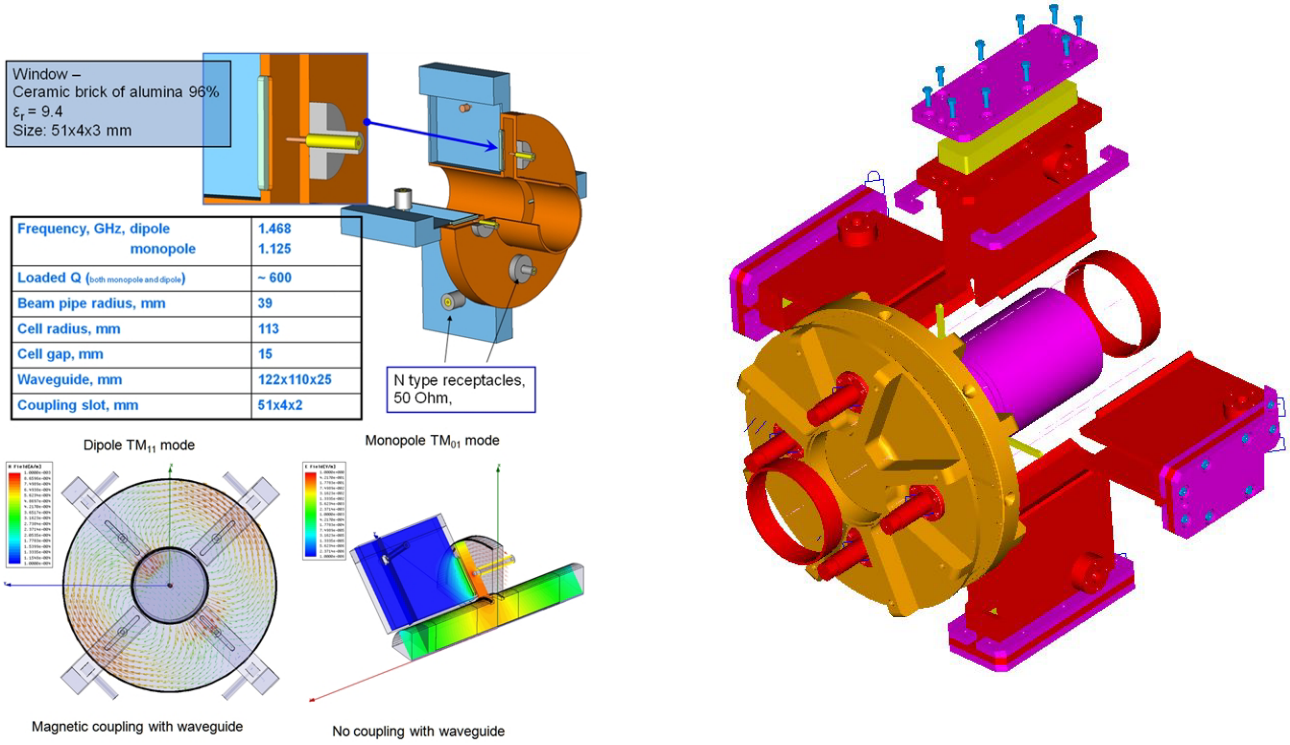

Figure 3.20: CM-free L-Band cavity BPM for the SRF cryostat.

3.3.8 Waveguide pickup

We propose this technique, as it is a quite simple and inexpensive technique to estimate the bunch length and verify the bunch compression.

The frequency domain magnitude spectrum of the beam is observed at a radiating ceramic gap at several (2-4) frequencies. Horn-antennas, waveguides, and detector elements are commercially available in a range 90-900 GHz. Similar experiments were executed at the SLAC Endstation-A [17] (Figure 3.21) and at the CERN CLIC Test Facility [18]. The response time of the detector elements is <<1 ns and the noise characteristics are excellent, thus allowing single bunch measurements. The setup is very simple and straightforward, however an absolute calibration of the bunch length is extremely difficult (no phase information, unknown insertion loss, and unknown sensitivity among the different frequency channels). However, this simple, inexpensive method gives a non-invasive, relative observation of the length of each single bunch.

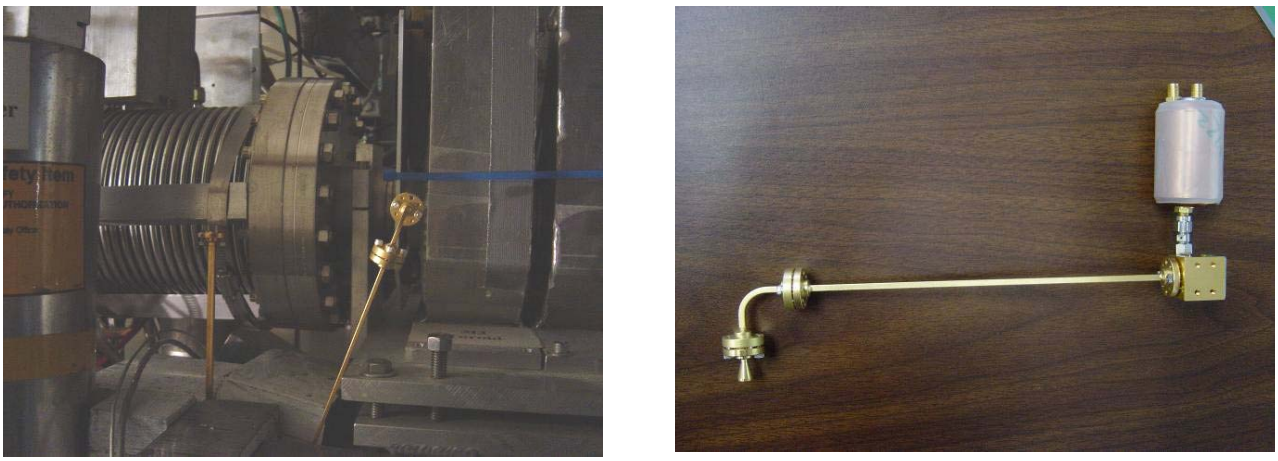

Figure 3.21: 300 GHz waveguide pickup system tested at SLAC ESA.

References

[1] R. Akre *et al.*, in *Proc. PAC2001, Chicago, IL*, p. 2353; R. Akre et al, Phys. Rev. ST Accel. Beams **11**, 030703 (2008).

[2] B. Beutner, Ph.D Thesis, University of Hamburg (2007).

[3] G. Berden, *et al.*, Phys. Rev. Lett. **99**, 164801 (2007).

[4] S. P. Jamison, *et al.*, TUYPA01, in *Proc. EPAC2006, Edinburgh, Scotland*.

[5] A. L. Cavalieri, *et al.*, Phys. Rev. Lett. **94**. 114801 (2005).

[6] J. Corbett *et al.*, in *Proc. PAC2007, Albuquerque, NM*, FRPMS065, p. 4159.

[7] A. Lumpkin, J. Ruan, "Initial Synchroscan Streak Camera Imaging at the A0 Photoinjector", submitted to *Proc. BIW2008, Lake Tahoe, CA*, (to be published).

[8] R. Thurman-Keup, *et al.*, TUPTPF015, in *Proc. BIW2008, Lake Tahoe, CA, USA*.

[9] F. Loehl, THOBF101, in *Proc. EPAC2006, Edinburgh, Scotland*.

[10] F. Loehl, WG506, in *Proc. Future Light Source 2006, Hamburg, Germany*.
[11] G. Kazakevich, *et al.*, FRPMN062, in *Proc. PAC2007, Albuquerque, NM, USA*.
[12] A.G. Shkvarunets, R. B. Fiorito, Phys. Rev. ST Accel. Beams **11**, 012801 (2008).
[13] A. G. Shkvarunets, *et al.*, WEPC21, in *Proc. DIPAC2007, Venice, Italy*.
[14] S. Molloy, *et al.*, Phys. Rev. Lett. **9**, 112802 (2006).
[15] S. Molloy, *et al.*, THOAC03, in *Proc. PAC2007, Albuquerque, NM, USA*.
[16] A. Lunin, *et al.*, TUPC23, in *Proc. DIPAC2007, Venice, Italy*.
[17] S. Molloy, *et al.*, FRPMS073, in *Proc. PAC2007, Albuquerque, NM, USA*.
[18] T. Levefre, *et al.*, WEIOTIO02, in *Proc. BIW2008, Lake Tahoe, CA, USA*.

4 Facility upgrades

4.1 RF gun

The gun and cathode chamber will be replaced by newer versions from DESY and INFN Milano, respectively. The new cathode chamber will allow for easier changing of the cathodes and the ability to prepare cathodes outside of the beamline cave. The new gun with its on-axis coaxial input coupler will improve gun operation, and reduce dark current, breakdown, and emittance.

In conjunction with the TESLA collaboration, Fermilab has constructed and operated several L-band (1.3 GHz) photo-cathode RF guns. One of these guns is presently installed at the A0PI, while another gun was installed at the DESY TTF. Both these Fermilab-built guns have exhibited deficiencies, most notable RF break-downs at long pulses caused by excessive heating at the input coupler slot. Dark current has also been an issue but this is more likely a feature of the cathode than of the gun. The gun at the DESY TTF was later upgraded with a new RF gun, while the Fermilab gun has remained in operation. Fermilab has recently obtained all documentation needed to produce this new upgraded RF gun. This DESY-type RF gun will be procured, commissioned and installed at the A0PI as part of the upgrade. It is schematically shown in Figure 4.1. The DESY-type gun has been characterized at DESY Zeuthen PITZ [1] where they measured normalized 90% emittances of ~1.5 mm-mrad at 1 nC. The normalized 90% emittance measured at the end of the 120 MeV injector at DESY is ~2 - 2.5 mm-mrad with 3MW gun rf power. These measurements give us some expectation that we may improve our beam emittance after the new gun (and, possibly, capture cavity) are installed. RF power for the gun will remain the same as at present (3 MW) and limit the gradient on the cathode to about 35 MV/m. Table 4.1 summarizes the main parameters of the RF gun.

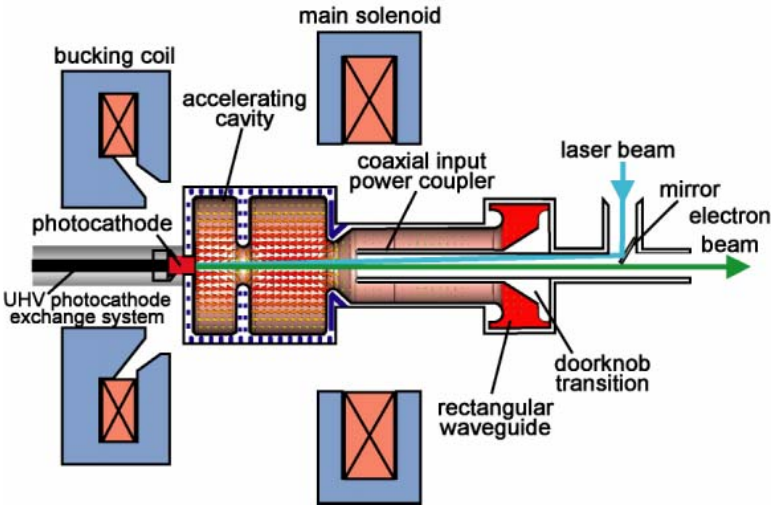

Figure 4.1: Schematic of the DESY-type RF photo gun.

Table 4.1**:** The main RF gun parameters

electrons/bunch	2×10^{10}
bunches/pulse	up to 3000
bunch repetition rate	3 MHz
pulse repetition rate	up to 5 Hz
average current	50 μA
beam energy	4.5 MeV
RMS bunch length	1 – 6 mm
RMS normalized emittance	4-5 μm

The difference in design between the Fermilab and the DESY guns will require the following other components to be replaced at the A0PI: (1) the gun cavity itself, (2) the focusing solenoids, (3) the coaxial RF coupler, (4) the laser mirror cross, and (5) the cathode exchange system. The current drive laser system will be replaced by a Ti:Sapphire based system, as discussed in Sections 2.2 and 3.2 of this proposal.

4.2 SRF acceleration cavity

At the current beam energy of 16 MeV space charge effects play a significant role in the beam dynamics. Increasing the beam energy to ~30 MeV will reduce space charge effects by a factor ~4. The current accelerating cavity has a low quench threshold and is limited to ~12 MV/m. There exists an additional, similar accelerating cavity and cryomodule which is being installed at NML solely to provide a cryogenic load to commission the new cryogenic system there. This cavity is capable of a gradient of ~25 MV/m. After the NML cryogenic system is commissioned, there will be the opportunity to move this higher gradient cavity to the A0PI, replacing the current low-gradient cavity and accomplishing the energy upgrade to ~30 MeV. This replacement would also provide the opportunity to repair the low-gradient cavity before it is installed at NML. Preliminary simulations indicate that reasonable transverse beam emittance is achievable at ~30 MeV with a single accelerating cavity (Figure 4.2).

Implementation of this upgrade is still under consideration, but would take place at the same time the RF gun is replaced. Most likely this will be in early Summer of 2009.

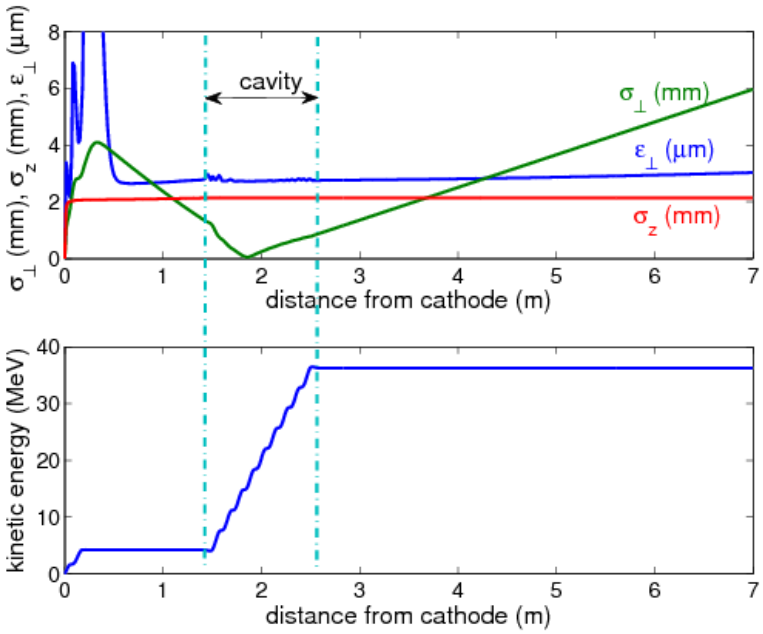

Figure 4.2**:** Beam parameters evolution with a 25 MV/m accelerating cavity. Beam transverse rms size, emittance and bunch length (top) and kinetic energy (bottom) are shown. Egun peak E-field is 40 MV/m and charge per bunch is 1 nC.

4.3 Other components

Beamline reconfiguration

The accelerating cavity is followed by a round-to-flat beam transformer composed of three quadrupoles, a set of normal quadrupoles, and is then split into two lines. One line has a double dogleg configuration, and the other line currently is open. We will reconfigur this 2nd line as a magnetic chicane. Both lines have spectrometer dumps. (The current layout is shown in Figure 6.1.)

Low Level RF system

The present LLRF system coordinates and regulates the timing, RF phases and amplitudes of the three RF cavities and the laser. The systems are state-of-the-art FPGA-based regulation systems for each cavity. The approach is based on the developments at the DESY FLASH and XFEL facilities. Additional R&D and improvements to the system and controls interface are being implemented at Fermilab.

The A0PI provides a unique test bed for this ongoing development and improvement program as it is currently the only place at Fermilab where the systems and feedback algorithms can be rigorously tested with beam, as an integrated multi-cavity system.

Controls

The control and data acquisition system for the A0PI is based on the DOOCS (Distributed Object Oriented Control System) package from DESY. This package includes a framework for writing front-ends and a client for creating and displaying virtual control panels for operators. The client package is currently unsupported and a replacement is currently under development at DESY. We will upgrade to this replacement package if it proves suitable for A0PI operations.

Beam Monitor Read-out Systems

The read-out electronics systems for most basic beam monitors (e.g., toroids and beam position monitors) are outdated or temporary installations, unable to deliver the required performance and reproducibility of the beam parameters to be characterized. A new, low-cost 100 MS/s 8-channel VME digitizer, recently developed in-house, will replace old analog signal processing installations for beam position and intensity measurements. The BPMs will be equipped with a downconverter/calibration unit, already successfully tested at the ATF damping ring at KEK.

Radiation & Shielding

The radiation limit outside the cave is set to 1 mrem/hr and on the roof of the cave to 5 mrem/h. At the present 16 MeV operating energy an administrative beam current limit of 300 nC/sec applies. The existing enclosure shielding thickness is 320 gm/cm^2. At the higher energy of 30 MeV, we will have to determine the allowable pulse length and bunch charge to stay within the above limits. Minor improvements in shielding may be required.

SRF R&D

The A0 building supports an ongoing SRF research area with clean room, clean assembly area, high pressure rinse system and vertical dewar testing. Continued research and testing is planned for the area and the A0 technicians support both this activity and A0PI operations. The A0 area is the ideal place to test small special research cavities such as special coatings, single crystal special cavities, alternative processing, etc. Tests of both 1.3 and 3.9 GHz cavities take place here.

4.4 Collaborations and students

The A0PI has an extensive history of collaboration with other groups and institutions. Much of the hardware that makes up the photoinjector has come from other groups, and people from other institutions have spearheaded or been involved with both the specific projects and the hardware or equipment that make up the photoinjector. These collaborative activities are summarized in Table 4.2.

At present Argonne, Northern Illinois University, Fermilab, and University of Chicago are collaborating in a partnership-like arrangement where we try to supplement each of the other's activities and build on the interchange of both ideas and utilization of equipment and resources. We are hoping to enlarge this group to include participation from others such as University of Maryland, University of Wisconsin, and MIT. At present, discussions of possible mutual interest are in initial phases. We believe we have a facility that well complements that at Maryland and student studies of photoinjector issues and diagnostic development of short bunches could complement their activities. Both Wisconsin and MIT are interested in participating in the ellipsoidal beam experiment and have also expressed interest in electron-laser interactions.

Collaboration continues with DESY and INFN Milano on RF gun development.

Table 4.2: Collaborating and participating institutions, past and present.

institution	equipment	projects/people
Argonne		emittance exchange, EOS
Cornell	4 MW klystron, SRF equipment	ILC fast kicker and tests
DESY	TESLA SRF cavities CC1 and CC2, 300 kW klystrons, RF guns, LLRF, DOOCS controls, Martin-Puplett interferometer	Flat beam
Fermilab		all
LBNL		Flat beam
INFN Frascati	intensified camera (loan)	student and use of camera
INFN Milano	cathode preparation chambers	commissioning of cathode systems
NIU	helium gas recovery system, laser oscillator	electro-optical imaging
Rutgers		emittance exchange, CC2 install and test
Saclay/Orsay	SRF cavity cryostats, tuner	injector characterization
UCLA	plasma chamber, magnets	plasma wakefield acceleration and focusing, photoinjector design
Univ. of Chicago		Flat beam
Univ. of Illinois		ILC fast kicker, students and tests
Univ. of Rochester	drive gun laser and additional equipment	Laser assembly, commissioning, EOS, laser acceleration, two macrobunch compression

Students and their supervision are a specific issue for the A0PI. A list of past and present PhD students is given in Table 4.3. For the activities at A0 to be effective there must be a critical mass including both staff and students. We must find stable student sources in order to have a viable program. In the past many of the students have come from University of Rochester and UCLA. We look forward to students from NIU and Chicago, but we must establish other strong university connections.

Table 4.3: Past and current graduate students at the A0PI.

name	institution	date of PhD	thesis topic	current institution
Eric Colby	UCLA	1997	RF photoinjector gun	SLAC
Alan Fry	Univ. of Rochester	1998	laser development	
Mike Fitch	Univ. of Rochester	2000	electro-optical sampling	
Jean-Paul Carneiro	Universite Paris XI	2001	experimental studies of photoinjector	Fermilab
Yin-e Sun	Univ. of Chicago	2005	flat beam transform	Fermilab
Matt Thompson	UCLA	2005	plasma acceleration	
Rodion Tikhoplav	Univ. of Rochester	2006	laser acceleration	UCLA
Tim Koeth	Rutgers Univ.	current	emittance exchange	
Artur Paytyan	Yerevan Univ.	current	SC RF controls	
Timothy Maxwell	NIU	current	EO imaging	

References

[1] Phys. Rev. ST Accel. Beams **9**, 092802 (2006); WEPPH008, in *Proc. FEL2007, Novosibirsk, Russia*.

5 Transition to Mid-West AARD Center (NML)

The Tesla Test Facility at DESY has provided a valuable system test for many elements of the TESLA SRF technology. However, several important changes to the TESLA RF cavity and cryomodule design are being planned for the ILC and for Project X at Fermilab. These will include a higher cavity gradient, relocation of the quad, shortening of the cavity end-group, and a new tuner design. Such changes will likely be introduced in several steps, with the first one being called a Type-IV cryomodule design. Also under discussion are different modulators, klystrons, cavity shapes, and other devices related to cryomodule operation. The minimum size system test needed to confirm the performance of such a new design for Project X is 2 cryomodules with 9 mA beam current per pulse.

Presently, Fermilab is building an ILC / Project X test facility, called NML, at the existing New Muon Lab building (Figure 5.1). NML will be the only U.S. facility capable of testing completed cryomodules, and this facility will be capable of testing cryomodules at high accelerating gradients with an ILC-like beam. NML will perform the initial tests of Type-IV cryomodules, and the goal is to produce and test 2 full cryomodules by the end of FY11. This facility will be invaluable to the SRF R&D program leading up to and most likely through the Project X construction. It will allow for a dedicated study of dark currents, HOM extraction, alignment, LLRF and control issues, cryogenic issues, RF power distribution, reliability and system recovery issues. Although the SRF program will be the first user of this facility, it will not be the only user. As the need for SRF-related tests diminishes, the facility will increase service to other users, such as the Advanced Accelerator R&D projects and experiments.

Figure 5.1: Photograph of interior of NML building, looking towards future high energy end. Visible is a single cryomodule (yellow).

The NML test facility will consist of the injector area comprised of the electron gun, acceleration cavities, and low energy beamlines (~24 m), the accelerator area comprised of 2 cryomodules (~27 m), and the high energy beamlines and dump area (~22 m). A schematic layout is shown in

Figure 5.2. Currently, a temporary cryogenics system is being installed in the building, but a new cryogenics plant will be added to the facility in the future in order to accommodate the correct fluid temperatures and to provide higher cryogenic capacities.

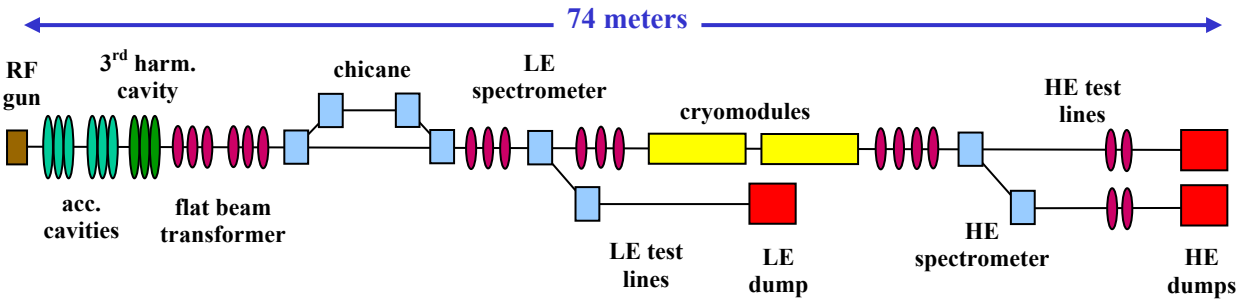

Figure 5.2: Approximate layout of NML beamlines.

Eventually the NML building may be extended so that additional cryomodules can be accomodated and also to add additional space for an enlarged AARD program in the high energy beamlines. The injector will provide beam energies up to 50 MeV and the high energy beamlines will provide energy >500 MeV (with 2 cryomodules). The experiments presented in this proposal can be continued at NML, and in addition, the following experiments have been discussed:

- ILC crab cavity tests
- Optical stochastic cooling
- in-vacuum laser acceleration
- beam driven acceleration in slab dielectric structures
- development of optical diffractive radiation diagnostics.

6 Appendices

6.1 Parameters

Table 6.1: Current A0PI beam parameters

parameter	units	value
gun gradient @ cathode	MV/m	35-40
9-cell cavity accelerating gradient	MV/m	12
bunch spacing	μs	1
# of bunches/pulse		10 - 200
RF pulse length	μs	30 - 300
pulse repetition rate	Hz	1
cathode efficiency	%	0.5 -2.0
laser UV energy	μJ/bunch	16
FWHM laser pulse length, unstacked/stacked	ps	5/21
bunch charge	nC	1 - 10 typ.
kinetic energy after gun	MeV	4.0
kinetic energy after 9-cell cavity	MeV	16
gun solenoid peak field	Gauss	1200
laser spot radius @ cathode	mm	0.7 - 1.6
RMS normalized emittance @ 1 nC	10^{-6}m	4-6
RMS normalized emittance @ 8 nC	10^{-6}m	12.6
uncompressed beam		
RMS momentum spread @ 16 MeV @ 1 nC	%	0.25 - 0.38
RMS bunch length @ 1 nC	mm	1.6
RMS bunch length @ 8 nC	mm	2.9
peak bunch current	A	75 - 330
bunch compressor		
Compressor R56	cm	8
Compressor Max. Dispersion	cm	14
Compression Phase	degrees off crest	-39
Chirped Energy spread	%	1.32
Compressed Bunch Length @ 1nC	mm	0.21
peak bunch current	A	1400
double dogleg compressor		
Compressor R56	cm	24
Compressor Max. Dispersion	cm	66
Compression Phase	degrees off crest	-20
Compressed Bunch Length @ 1nC	mm	0.19
peak bunch current	A	1570
emittance exchange		
CC1 Phase	degrees off crest	-20
Beam Energy	MeV	14.3
Energy Spread	%	0.8
Bunch Length	mm	0.45

Table 6.2 Current A0PI drive laser parameters

parameter	units	value
oscillator frequency	MHz	81.25
oscillator wavelength	nm	1054
oscillator energy/pulse	nJ	5.5
energy/pulse after multi-pass	μJ	6
energy/pulse after two-pass	μJ	100
UV energy/pulse after crystals	μJ	20
UV energy/pulse on cathode	μJ	10
UV pulse length (FWHM)	ps	5
pulse separation	μs	1
length of pulse train		up to 800 bunches
train repetition rate	Hz	1

6.2 Facility layout

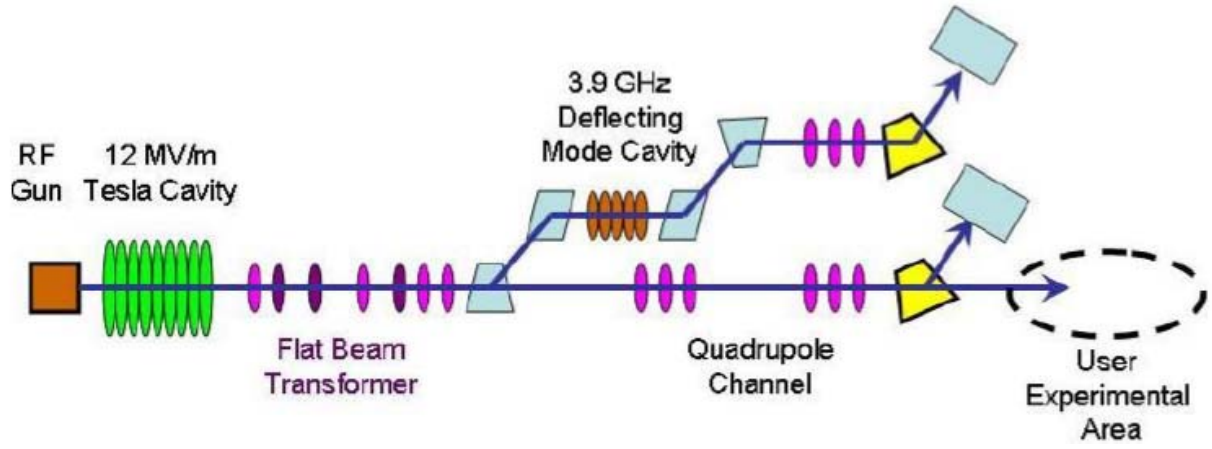

Figure 6.1: Current A0PI layout.